JACS
JOURNAL OF THE AMERICAN CHEMICAL SOCIETY

ARTICLE

pubs.acs.org/JACS

Synthesis of Aluminosilicate and Gallosilicate Zeolites via a Charge Density Mismatch Approach and Their Characterization

Min Bum Park,[†] Sung June Cho,[‡] and Suk Bong Hong*[,†]

[†]Department of Chemical Engineering and School of Environmental Science and Engineering, POSTECH, Pohang 790-784, Korea, and [‡]Department of Applied Chemical Engineering, Chonnam National University, Kwangju 500-757, Korea

Supporting Information

ABSTRACT: Aluminosilicate and gallosilicate zeolite syntheses via a charge density mismatch (CDM) approach are compared at intermediate-silica compositions (Si/Me = 5−16, where Me is Al or Ga). With a variation of the crystallization temperature and of the type and/or concentration of alkali metal ions added as a crystallization structure-directing agent (SDA) to tetraethylammonium−tetramethylammonium, tetraethylammonium−hexamethonium, and strontium−choline mixed-SDA systems, we were able to obtain 11 different zeolite structures. However, only 5 out of a total 40 pairs of aluminosilicate and gallosilicate synthesis runs at otherwise identical chemical compositions were found to give the same zeolite product with no detectable impurities, suggesting that the structure-directing ability of Ga is quite different from that of Al even in intermediate-silica synthesis conditions. The CDM approach to offretite synthesis led to hexagonal plate-like crystals with aspect ratios lower than 0.3, and UZM-22 exhibited no significant preference of Al substitution for particular tetrahedral sites, especially for site T1, unlike its framework type material ZSM-18. More interestingly, the EU-1 zeolite obtained from an aluminosilicate synthesis mixture containing Li^+ as an inorganic crystallization SDA in the tetraethylammonium−hexamethonium double-organic additive system has been characterized to locate about half of its Li^+ ions in the framework, while the Li distribution over the 10 topologically different tetrahedral sites is nonrandom in nature.

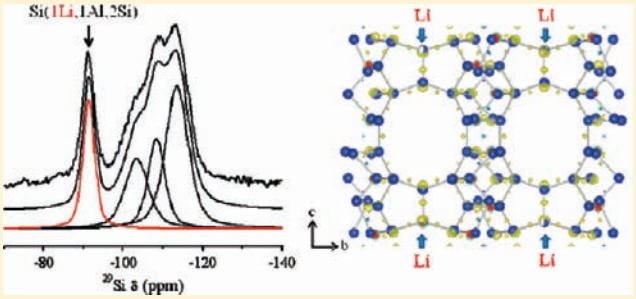

INTRODUCTION

Zeolite synthesis is still an active field of research because previously unobserved zeolites and zeolite-like materials are potentially useful for finding new applications not only in ion exchange, separation, and catalysis but also in nontraditional areas such as device and medical technologies.[1] It was in the early 2000s when researchers at UOP developed a charge density mismatch (CDM) approach in an attempt to force a cooperative structure direction with double or multiple structure-directing agents (SDAs) during the crystallization process of zeolites. Before long, this clever strategy allowed them to discover UZM-5 (framework type UFI), a new cage-based small-pore zeolite, together with several other materials with known framework structures but unprecedented chemical compositions such as UZM-4 (BPH), UZM-9 (LTA), UZM-12 (ERI), and UZM-22 (MEI),[2] which confirms a certain degree of rational design. The essential feature of the CDM approach lies in the preferred formation of synthesis mixtures in which a large mismatch in the charge density and spatial correspondence exits between the organic SDA and the pore architecture arises, making it practically impossible to induce zeolite crystallization. Therefore, the addition of a supplementary SDA with a higher charge density at much lower levels, frequently at substoichiometric ones, compared to Al in CDM synthesis mixtures is required to overcome this situation.

The CDM approach was first applied to the aluminosilicate system in which only organic additives (e.g., tetraethylammonium or tetrapropylammonium) with a low charge density were included as a main SDA. Then, it was successfully expanded through the additional use of organic SDAs with a higher charge density, alkali metal, and/or alkali earth metal cations as crystallization SDAs in the presence of one or more organic SDAs. We have recently investigated details of the CDM approach to zeolite syntheses and shown that the phase selectivity of the crystallization differ notably according not only to the synthesis temperature but also to the type of alkali cations added as an inorganic crystallization SDA to the synthesis mixture.[3] On the other hand, isomorphous substitution of Al and/or Si by other elements such as Li, Be, B, Zn, and Ge in zeolite frameworks during the crystallization process is one of the rational strategies for synthesizing previously unobserved topologies, as well as for

Received: October 21, 2010
Published: January 19, 2011

Table 1. Representative Synthesis Conditions[a] and Results

SDA system no.	synthesis mixture composition[b]	M	product[d] T = 100 °C Me = Al	T = 100 °C Me = Ga	T = 150 °C Me = Al	T = 150 °C Me = Ga
I	8TEAOH:0.5TMACl: 0.5MCl:0.5Me_2O_3:8SiO_2:240H_2O	Li	Li-Al-UZM-9	L	Li-Al-beta + Li-Al-UZM-5	L
		Na	Na-Al-UZM-9	Na-Ga-offretite(I)	Na-Al-UZM-5	amorphous
		K	K-Al-offretite(I)	K-Ga-offretite(I)	amorphous	amorphous
		Rb	−[e]	Rb-Ga-offretite(I)	−[e]	amorphous
		Cs	Cs-Al-offretite(I)	Cs-Ga-analcime(I)	amorphous	amorphous
II	8TEAOH:0.5TMACl: 1.5MCl:0.5Me_2O_3:8SiO_2:240H_2O	Li	Li-Al-sodalite + L	L	Li-Al-beta + Li-Al-sodalite + L	Li-Ga-beta + Li-Ga-sodalite + L
		Na	Na-Al-offretite(II)	Na-Ga-omega	Na-Al-omega + Na-Al-ZSM-12	Na-Ga-omega + Na-Ga-ZSM-12
		K	K-Al-offretite(II)	K-Ga-merlinoite + K-Ga-offretite(II)	K-Al-ZSM-12 + amorphous	K-Ga-offretite(II) + K-Ga-ZSM-12
		Rb	Rb-Al-merlinoite	Rb-Ga-beta + Rb-Ga-omega	Rb-Al-merlinoite + Rb-Al-ZSM-12	Rb-Ga-beta
		Cs	−[e]	Cs-Ga-analcime(II)	Cs-Al-analcime(II)	Cs-Ga-analcime(II)
III	6.5TEAOH:1$HMBr_2$: 0.75MCl:0.25Me_2O_3:8SiO_2:240H_2O	Li	L	L	Li-Al-EU-1	L
		Na	amorphous	−[e]	amorphous	−[e]
		K	K-Al-UZM-12	K-Ga-UZM-12	K-Al-UZM-12 + U	K-Ga-EU-1
		Rb	Rb-Al-UZM-12	Rb-Ga-UZM-12	Rb-Al-UZM-12 + U	Rb-Al-analcime(III) + U
		Cs	Cs-Al-analcime(III)	amorphous	Cs-Al-EU-1 + amorphous	amorphous + U
IV	6.4ChOH:0.24MCl: 0.24$Sr(NO_3)_2$:0.8Me_2O_3:8SiO_2:240H_2O[c]	Li	Li-Al-UZM-22	−[e]	Li-Al-sodalite	amorphous
		Na	Na-Al-UZM-22	−[e]	Na-Al-sodalite	amorphous
		K	K-Al-offretite(IV)	K-Ga-offretite(IV)	amorphous	amorphous
		Rb	Rb-Al-UZM-22	Rb-Ga-offretite(IV)	Rb-Al-sodalite	amorphous
		Cs	Cs-Al-UZM-22	amorphous + Cs-Ga-offretite(IV)	amorphous + Cs-Al-UZM-22	Cs-Ga-sodalite

[a] All the syntheses were performed using $Al[OCH(CH_3)C_2H_5]_3$ as an Al source under rotation (60 rpm) at 100 or 150 °C for 14 days, unless otherwise stated. [b] TEA, TMA, HM, and Ch represent tetraethylammonium, tetramethylammonium, hexamethonium, and choline ions, respectively. [c] $Al(OH)_3 \cdot H_2O$ was used as an Al source. [d] The product appearing first is the major phase. L and U indicate layered and unknown phases, respectively. [e] No solids were obtained.

manipulating their physicochemical and catalytic properties for specified applications.[4] This is also the case for Ga, the element most chemically similar to Al, given the discovery of gallosilicate zeolites TsG-1/ECR-9/TNU-1 (CGS) and ECR-34 (ETR) which have no counterpart among aluminosilicates.[5,6] Hence, there is an increasing consensus that the structure-directing ability of Ga could be substantially different from that of Al in certain low-silica (Si/Me ≤ 5, where Me is Al or Ga) synthesis conditions.[7]

The purpose of this work is to compare the structure-directing ability of Ga with that of Al under four different CDM synthesis conditions in which the Si/Me ratio is varied between 5 ≤ Si/Me ≤ 16 and thus lies at intermediate-silica compositions. Here we have carried out a total of 40 pairs of aluminosilicate and gallosilicate synthesis runs at otherwise identical chemical compositions in tetraethylammonium−tetramethylammonium, tetraethylammonium−hexamethonium, and strontium−choline mixed-SDA systems which had been previously used in the synthesis of UZM-5 or UZM-9, UZM-12, and UZM-22, respectively.[2,3] The materials obtained are characterized by using powder X-ray diffraction, elemental and thermal analyses, scanning electron microscopy, N_2 sorption, IR, multinuclear MAS NMR, and ^{27}Al MQ MAS NMR. In particular, the crystal structure of the as-made form of EU-1 (EUO) prepared using a lithium aluminosilicate synthesis mixture in the tetraethylammonium−hexamethonium double-organic additive system has been determined by the Rietveld analysis of its synchrotron diffraction data in order to confirm not only the substitution of Li atoms into the EU-1 framework but also the nonrandom nature of their distribution over the 10 crystallographically different tetrahedral sites (T-sites).

dx.doi.org/10.1021/ja1095057 |J. Am. Chem. Soc. 2011, 133, 1917–1934

EXPERIMENTAL SECTION

Synthesis. Four mixed-SDA systems with different synthesis mixture compositions as listed in Table 1 were used in zeolite syntheses. The CDM aluminosilicate and gallosilicate mixtures were prepared by combining aluminum tri-*sec*-butoxide ($Al[OCH(CH_3)C_2H_5]_3$, 97%, Aldrich) or aluminum hydroxide ($Al(OH)_3 \cdot 1.0H_2O$, Aldrich) and gallium oxide (Ga_2O_3, 99.99+%, Aldrich) as Al and Ga sources, respectively, with tetraethylammonium hydroxide (TEAOH, 35% aqueous solution, Aldrich) or choline hydroxide (ChOH, 20% aqueous solution, Aldrich) and water followed by the addition of colloidal silica (Ludox AS-40, DuPont). The mixtures were then heated overnight at 95 °C. To the resulting clear solutions, after being cooled to room temperature, tetramethylammonium chloride (TMACl, 97%, Aldrich) or hexamethonium bromide ($HMBr_2$, 98%, Acros) was added as an organic crystallization SDA in conjunction with the chloride or nitrate of alkali metal (Li^+, Na^+, K^+, Rb^+, and Cs^+) or alkali earth metal (Mg^{2+}, Ca^{2+}, Sr^{2+}, and Ba^{2+}) cations. After being stirred at room temperature for 1 day, the final synthesis mixtures were charged into Teflon-lined 23-mL autoclaves and heated at 100 or 150 °C under rotation (60 rpm) for 14 days. If required, they were introduced into new Teflon liners that had never been in contact with a solution containing any alkali metal cation (M^+) to examine the effects of a small but nonnegligible amount of K^+ ions adsorbed on used liners on the phase selectivity of the crystallization. In addition, some synthesis experiments were carried out for periods of crystallization times up to 28 days. The solid products were recovered by filtration or centrifugation, washed repeatedly with distilled water, and dried overnight at room temperature. As-made zeolites were calcined in air at 550 °C for 8 h to remove the organic SDAs occluded. The calcined materials were then refluxed twice in 1.0 M NH_4NO_3 solutions for 6 h followed by calcination at 550 °C for 4 h in order to ensure that they were completely in their proton form.

All zeolites prepared here were referred to as the following scheme: A-B-C, where the letters A, B, and C indicate the types of the inorganic cation and trivalent, tetrahedral lattice-substituting component added to the synthesis mixture, and the general name of zeolite produced, respectively. Unlike the other zeolitic phases, on the other hand, offretite (OFF) and analcime (ANA) were found to purely crystallize from more than one mixed-SDA system. Thus, the SDA system number (Table 1) was attached in parentheses to their names.

For structural comparison, an EU-1 zeolite with Si/Al = 26 was prepared according to the conventional procedure that includes the use of Na^+ and HM^{2+} as SDAs.[8] Here we refer to this EU-1 zeolite as Na-Al-EU-1.

Analytical Methods. Powder X-ray diffraction (XRD) patterns were recorded on a PANalytical X'Pert diffractometer (Cu Kα radiation) with an X'Celerator detector. Data were collected with a fixed divergence slit (0.50°) and Soller slits (incident and diffracted = 0.04 rad). For the calculation of the unit cell parameters, long-step scans were taken in the 2θ range 3−90° with a step width of 0.0084° and a scanning speed of 2.13° min^{-1}. Indexing of the powder XRD patterns obtained was carried out using the Highscore Plus program.[9] Elemental analysis for Si, Al, Ga, and alkali metal cations was carried out by a Jarrell-Ash Polyscan 61E inductively coupled plasma spectrometer in combination with a Perkin-Elmer 5000 atomic absorption spectrophotometer. The C, H, and N contents of the samples were analyzed by using a Vario EL III elemental organic analyzer. Thermogravimetric analyses (TGA) were performed on an SII EXSTAR 6000 thermal analyzer, where the weight losses related to the combustion of organic SDAs were further confirmed by differential analyses (DTA) using the same analyzer. Crystal morphology and average size were determined by a JEOL JSM-6510 scanning electron microscope (SEM). The N_2 sorption experiments were performed on a Mirae SI nanoPorosity-XG analyzer. The IR spectra in the structural region were recorded on a Midac M2000 FT-IR spectrometer using the KBr pellet technique. The IR spectra in the C−H and O−H stretching regions were measured on the same spectrometer using self-supporting zeolite wafers. Prior to IR experiments, the zeolite wafers were dehydrated under vacuum to a residual pressure of 10^{-3} Torr overnight at 200 °C inside a home-built IR cell with CaF_2 windows. Then, the IR spectra were recorded under flowing N_2 at different temperatures. Typically, 256 scans were accumulated.

Multinuclear MAS NMR measurements were performed mainly on a Varian Inova 300 spectrometer at a spinning rate of 6.0 kHz. The ^{13}C MAS NMR spectra were recorded at a ^{13}C frequency of 75.428 MHz with a $\pi/2$ rad pulse length of 7.0 μs, a recycle delay of 2 s, and an acquisition of ca. 10 000 pulse transients. The $^1H-^{13}C$ CP MAS NMR spectra were obtained with an acquisition of ca. 5000 pulse transients, which was repeated with a contact time of 2.5 ms and a recycle delay of 3 s. The ^{29}Si MAS NMR spectra were measured at a ^{29}Si frequency of 59.590 MHz with a $\pi/2$ rad pulse length of 5.0 μs, a recycle delay of 30 s, and an acquisition of about 5000 pulse transients. The ^1H MAS NMR spectra were recorded at a ^1H frequency of 299.945 MHz. The spectra were obtained with an acquisition of 64 pulse transients, which was repeated with a $\pi/2$ rad pulse length of 3.0 μs and a recycle delay of 0.5 s. The ^{13}C, ^{29}Si, and ^1H chemical shifts are reported relative to TMS. The ^{27}Al MAS NMR spectra were measured at a ^{27}Al frequency of 78.156 MHz with a $\pi/8$ rad pulse length of 1.8 μs and a recycle delay of 0.5 s. Approximately 3000 pulse transients were accumulated, and the ^{27}Al chemical shifts are reported relative to an $Al(H_2O)_6^{3+}$ solution. The ^{71}Ga MAS NMR spectra were recorded at a ^{71}Ga frequency of 91.468 MHz with a $\pi/2$ rad pulse length of 10 μs, a recycle delay of 30 ms, and an acquisition of ca. 20 000 pulse transients. The ^{71}Ga chemical shifts are reported relative to a $Ga(H_2O)_6^{3+}$ solution. The ^7Li and $^1H-^{29}Si$ CP MAS NMR spectra were measured on a Varian Inova 600 spectrometer at a spinning rate of 20 kHz. The ^7Li MAS NMR spectra were obtained at a ^7Li frequency of 233.162 MHz with a $\pi/4$ rad pulse length of 3.0 μs, a recycle delay of 5.0 s, and an acquisition of ca. 500 pulse transients. The ^7Li chemical shifts are reported relative to a LiCl solution. The $^1H-^{29}Si$ CP MAS NMR spectra were recorded at a ^{29}Si frequency of 119.182 MHz with $\pi/2$ rad pulse length of 6.5 μs, a recycle delay of 6.5 s, a contact time of 3 ms, and an acquisition of ca. 10 000 pulse transients. The ^{27}Al Multiplex Soft-Pulse-Adding-Mixing (SPAM) 3Q MAS NMR spectra were recorded on a Bruker Avance 400 spectrometer in a rotor-synchronized fashion at a spinning speed of 14 kHz and a ^{27}Al frequency of 104.26 MHz with a recycle delay of 0.5 s by advancing the evolution time t_1 increments equal to the rotor period.[10] The shearing procedure was systematically applied to each 2D spectra, and further details of the experimental conditions are described elsewhere.[11] All spectral deconvolution and simulation were performed using the PeakFit curve-fitting program.

For detailed structural analysis of two as-made aluminosilicate EU-1 zeolites synthesized using Li^+ as a crystallization SDA in the TEA^+-HM^{2+} mixed-organic SDA system and following the conventional procedure,[8] respectively, the synchrotron diffraction data were collected on the 8C2 beamline at Pohang Acceleration Laboratory (Pohang, Korea) using monochromatic synchrotron radiation (λ = 1.54940 Å). The detector arm of the vertical scan diffractometer consists of seven sets of Soller slits, flat Ge(111) crystal analyzers, antiscatter baffles, and scintillation detectors, with each set separated by 20°. Data were obtained on the sample at room temperature in flat plate mode, with a step size of 0.01° for a scan time of 10 s per step and overlaps of 2° to the next detector bank over the 2θ range 5−145°. The synchrotron diffraction patterns obtained were indexed using the DICVOL04 program implemented in the Fullprof suite of programs.[12] Profile refinement of the structure model, comprising the EU-1 framework

and including HM^{2+} molecules initially fixed at their energy-minimized locations determined by the MM2 method and parallel tempering algorithm,[13] was performed via the Rietveld method with the GSAS package.[14] Other extraframework species were not included. The profile was matched in the 2θ range 6.5−100° because of the large asymmetry of the first peak at low 2θ angle and the poor signal-to-noise ratio of the data at very high angles. During the Rietveld refinement, a pseudo-Voigt/FCJ function,[15] together with a manually interpolated background, was used to describe the peak shape. The framework was modeled as completely siliceous. Isotropic displacement parameters of all Si atoms were constrained to be equal to minimize the number of parameters, as were those of all O atoms and those of all SDA atoms. The data collection and crystallographic parameters are summarized in Supporting Information Table S1.

RESULTS AND DISCUSSION

Table 1 lists the representative products obtained from the four mixed-SDA systems with different oxide compositions under the synthesis conditions described above. In each case, the products listed were the only ones obtained in repeated trials. It can be seen that when the trivalent, tetrahedral lattice-substituting component is changed from Al to Ga at intermediate-silica compositions ($5 \leq Si/Me \leq 16$), most of the gallosilicate products are different from the aluminosilicate materials synthesized under otherwise identical conditions.

Our initial attempts to synthesize gallosilicate zeolites via a CDM approach were made to carry out the synthesis using Na^+ as an inorganic crystallization SDA after replacement of Al by Ga in the TEA^+-TMA^+ double-organic additive system where the crystallization of aluminosilicate UZM-9 proved to be highly reproducible.[2b,3a] As seen in Table 1, however, gallosilicate offretite was the phase crystallized after heating at 100 °C for 14 days. Although no alkali cations other than Na^+ were added to its synthesis mixture, elemental analysis reveals that this offretite contains a nonnegligible amount of K^+ (see below). Thus, it will be simply referred to as Na-Ga-offretite(I) according to the scheme described above. While replacement of Na^+ by the equivalent amount of K^+ or Rb^+ under the conditions identical to those for Na-Ga-offretite(I) formation led to no change in product, on the other hand, the use of Cs^+ gave gallosilicate analcime that could also be prepared in the absence of organic SDAs. Since this material is not the same as for the aluminosilicate product, i.e., Cs-Al-offretite(I), it appears that the phase selectivity of the crystallization in the TEA^+-TMA^+ system can vary with both the type of trivalent lattice-substituting components and alkali metal cations employed. As already reported,[2b,3a] in addition, the use of a sodium aluminosilicate synthesis mixture yielded UZM-5 instead of UZM-9 when the synthesis is performed at 150 °C. As seen in Table 1, however, the gallosilicate crystallization in the presence of Na^+ gave no zeolitic products. The same result was also obtained from synthesis mixtures containing any of the other four alkali cations as an inorganic crystallization SDA, indicating that crystallization temperature is another important phase selectivity factor.

The strong influence of the concentration of alkali cations in the synthesis mixture on the crystallization product has been frequently observed in zeolite syntheses, both with and without organic species present.[16] To check whether this trend is also evident in the CDM synthesis conditions, therefore, we increased the concentration of alkali cations three times in the TEA^+-TMA^+ mixed-organic SDA system while keeping other parameters constant and performed aluminosilicate and gallosilicate syntheses. When compared with the synthesis results obtained at a low level ($M^+/Me = 0.5$) of alkali concentration, 18 out of 20 runs preformed at a higher level ($M^+/Me = 1.5$) of concentration were found to yield different products although many of them appeared as mixed phases. When using sodium aluminosilicate and gallosilicate synthesis mixtures, for example, we always obtained offretite and omega (MAZ) after 14 days of heating at 100 °C, respectively. Also, the crystallization using a rubidium aluminosilicate synthesis mixture under the same conditions gave merlinoite (MER). At a higher crystallization temperature (i.e., 150 °C), by contrast, the use of a rubidium gallosilicate synthesis mixture led to the formation of zeolite beta (*BEA). Therefore, it is clear that the phase selectivity of the crystallization in the TEA^+-TMA^+ SDA system can also be altered according to the concentration of alkali metal cations added as an inorganic crystallization SDA to CDM synthesis mixtures, as well as to their type. However, there appears to be a marginal level of alkali concentration that can change the phase selectivity of the crystallization, because a further increase of M^+/Me ratio in the synthesis mixture from 1.5 to 3.0 gave no zeolite products except those already found in syntheses at lower ratios (i.e., 0.5 and 1.5).

As described earlier, UZM-12 and UZM-22 are two remarkable examples in which the CDM approach has successfully applied to the synthesis of aluminosilicate zeolites with already known framework structures but new chemical compositions. This led us to examine the structure-directing ability of Ga in their optimum synthesis conditions,[2,3] together with the effects of the type of alkali cations and the crystallization temperature on the framework structure of products. Unlike the case of UZM-5 or UZM-9, we were able to obtain both aluminosilicate and gallosilicate analogues of UZM-12 at 100 °C in the TEA^+-HM^{2+} mixed-SDA system. Under the synthesis conditions studied here, in fact, it was possible to crystallize UZM-12 zeolites containing Ga and Al atoms over the entire compositional range $0 \leq Ga/(Ga + Al) \leq 1$. As seen in Table 1, however, the crystallization of this ERI-type material was found to be sensitive to the type of alkali metal cations used as an inorganic crystallization SDA: replacement of K^+ or Rb^+ by the equal amount of Li^+, Na^+, or Cs^+ did not give UZM-12 at 100 °C. We also note that when the crystallization temperature is elevated to 150 °C, EU-1 was the product formed from lithium aluminosilicate or potassium gallosilicate synthesis mixture. This is not so surprising because HM^{2+} is the original organic SDA used in the synthesis of EU-1.[8]

Some changes in product caused by moving from Al to Ga can also be observed from the $Sr^{2+}-Ch^+$ SDA system. As already reported by UOP researchers,[2c] UZM-22 was the phase crystallized from an aluminosilicate synthesis mixture containing Li^+ or Na^+ as an inorganic crystallization SDA at 100 °C in this SDA system. However, the use of a gallosilicate synthesis mixture under otherwise identical conditions gave no solid products even after 28 days of heating. While such differences in the product of aluminosilicate and gallosilicate syntheses in the presence Rb^+ or Cs^+ and/or at a higher crystallization temperature (150 °C) were observed, we were able to obtain offretite from both potassium aluminosilicate and gallosilicate synthesis mixtures at 100 °C. Since the same result was found in the TEA^+-TMA^+ SDA system, it is most likely that the ability of K^+ to direct the

synthesis of offretite is more selective than that of any of the other four alkali cations. On the other hand, Wang et al. have recently reported that UZM-22 could be synthesized with the aid of either Li^+ or Sr^{2+} in the presence of Ch^+, although a considerably longer period of crystallization time is required.[17] This implies that the addition of either inorganic cation to the Ch^+-containing aluminosilicate synthesis mixture is not essential to the crystallization of UZM-22 but is beneficial to accelerate the rate of its nuclei formation and/or the rate of subsequent crystal growth. As seen in Table 1, in fact, pure UZM-22 could also be obtained using Rb^+ or Cs^+ instead of Li^+ in the $Sr^{2+}-Ch^+$ SDA system. Since the use of Ca^{2+} as a substitute of Sr^{2+} was found to give this unique large-pore zeolite after 28 days of heating at 100 °C, in addition, we believe that UZM-22 crystallization can be rationalized in terms of a cooperative structure-directing effect of Ch^+ and alkali or alkali earth cations.

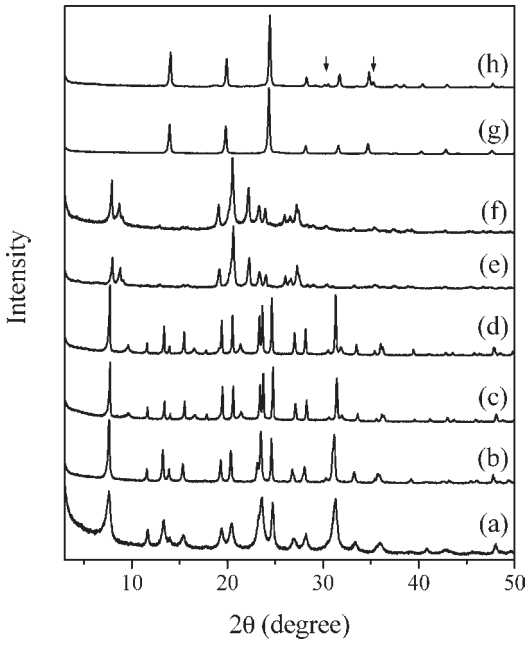

Figure 1. Powder XRD patterns of four representative pairs of as-made aluminosilicate and gallosilicate zeolites with different framework topologies prepared in this study: (a) K-Al-offretite(I), (b) K-Ga-offretite(I), (c) K-Al-UZM-12, (d) K-Ga-UZM-12, (e) Li-Al-EU-1, (f) K-Ga-EU-1, (g) Na-Al-sodalite, and (h) Cs-Ga-sodalite. The X-ray peaks from β-Ga_2O_3 are marked by arrows.

The synthesis results presented thus far have revealed that 11 different zeolite structures could be synthesized in the range of CDM synthesis conditions studied here, mainly depending on the type of alkali cations and trivalent, tetrahedral lattice-substituting components, as well as on the crystallization temperature. In particular, the fact that only 5 out of a total 40 pairs of aluminosilicate and gallosilicate synthesis runs at otherwise identical chemical compositions gave the same zeolite products with no detectable impurities suggests that the difference in the interactions of aluminosilicate and gallosilicate species with a particular type of alkali cations is large enough to affect the phase selectivity of the crystallization even at intermediate-silica compositions. In this regard, combining an adequate screening of inorganic and organic synthesis parameters with the structure-directing role of Ga in CDM synthesis conditions appears to be a viable approach in the search for novel intermediate-silica zeolite structures. It is also remarkable that although more than two dozen gallosilicate analogues of silica-based zeolites with different framework topologies have been synthesized thus far,[18] none of them contain double 4-rings (D4Rs) as a secondary building unit that are found in several aluminosilicate zeolites including zeolite A (LTA), UZM-5, ITQ-13 (ITH), and ITQ-27 (IWV).[2a,4f,19] The precise reason for this remains unclear, because the ratio (0.88) of nonbonded radius to T−O distance for Ga is even slightly lower than that (0.92) for Al.[20]

Figure 1 shows the powder XRD patterns of four representative pairs of as-made aluminosilicate and gallosilicate zeolites with different framework topologies prepared in this study. The XRD patterns of the other notable zeolites can be found in Supporting Information Figure S1. Comparison with the XRD patterns in the literature[21] reveals that all the materials are highly crystalline and no reflections other than those from each material, except Cs-Ga-sodalite (SOD) containing a trace amount of β-Ga_2O_3 as an impurity,[22] are observed. We also note that all the peaks from K-Ga-offretite(I) synthesized at a low Na^+/Me ratio of 0.5 in the TEA^+-TMA^+ SDA system (Table 1) are much narrower than those from its aluminosilicate analogue, i.e., the K-Al-offretite(I) material which is nanocrystalline in nature as recently reported.[3a] This is not unexpected because zeolite crystal size frequently becomes much larger upon isomorphous substitution of Al by Ga.[18]

Table 2. Crystallographic and Structural IR Data for Four Representative Pairs of As-Made Aluminosilicate and Gallosilicate Zeolites with Different Framework Topologies Prepared in This Study

			unit cell parameters and volume					IR band position, cm^{-1}	
material	IZA code	Si/Me[a]	*a*, Å	*b*, Å	*c*, Å	*V*, Å^3	ΔV,[b] %	ν_{as}(T-O)[c]	δ(T-O)[d]
K-Al-offretite(I)	OFF	3.15	13.304(7)		7.580(6)	1161.9	−	1041	464
K-Ga-offretite(I)	OFF	3.71	13.305(3)		7.602(2)	1165.4	0.3	1041	459
K-Al-UZM-12	ERI	4.74	13.152(3)		15.023(6)	2250.5	−	1068	474
K-Ga-UZM-12	ERI	5.39	13.250(3)		15.107(7)	2296.7	2.1	1055	463
Li-Al-EU-1	EUO	15.5	13.700(3)	22.321(6)	20.194(4)	6175.4	−	1084	466
K-Ga-EU-1	EUO	14.5	13.716(3)	22.303(7)	20.207(6)	6181.6	0.1	1084	463
Na-Al-sodalite	SOD	4.99	8.874(8)			698.8	−	1077	457
Cs-Ga-sodalite	SOD	4.30	8.879(7)			700.0	0.2	1072	457

[a] Determined from elemental analysis. [b] $\Delta V = 100 \times (V_{Ga} - V_{Al})/V_{Al}$, where V_{Ga} and V_{Al} are the unit cell volumes of the as-made gallosilicate and aluminosilicate counterparts of each zeolite structure, respectively. [c] Asymmetric T−O stretching mode, where T is Si, Al, or Ga. [d] T−O bending mode.

dx.doi.org/10.1021/ja1095057 |J. Am. Chem. Soc. 2011, 133, 1917–1934

Table 3. Chemical Composition Data for Selected Zeolites with Different Framework Topologies and/or Compositions Prepared Here

material	organic SDA(s) used	%N	%C	%H	%$\sum$[a]	C/N	unit cell composition[b]	Si/Me[c]	BET surface area, $m^2\ g^{-1}$ total	BET surface area, $m^2\ g^{-1}$ microporous	BET surface area, $m^2\ g^{-1}$ external
K-Al-offretite(I)	TEA^+, TMA^+	2.06	8.82	2.94	13.82 (14.1)	4.99	$\|TEA_{0.6}TMA_{1.7}Na_{0.2}K_{2.2}OH_{0.3}(H_2O)_{4.7}\|$ $[Al_{4.4}Si_{13.6}O_{36}]$	3.15 (2.92)	480	360	120
K-Ga-offretite(I)	TEA^+, TMA^+	1.70	7.82	2.42	11.93 (10.9)	5.33	$\|TEA_{0.7}TMA_{1.4}Na_{1.7}K_{2.0}OH_{1.9}(H_2O)_{9.7}\|$ $[Ga_{3.8}Si_{14.2}O_{36}]$	3.71 (3.23)	420	390	30
Na-Ga-offretite(I)	TEA^+, TMA^+	1.57	6.60	2.48	10.66 (11.3)	4.85	$\|TEA_{0.4}TMA_{1.5}Na_{1.5}K_{0.9}OH_{0.4}(H_2O)_{10.6}\|$ $[Ga_{3.9}Si_{14.1}O_{36}]$	3.58 (3.18)	400	390	10
Na-Al-offretite(II)	TEA^+, TMA^+	1.34	4.93	2.58	8.85 (10.0)	4.27	$\|TEA_{0.1}TMA_{1.6}Na_{2.9}K_{0.5}OH_{0.2}(H_2O)_{7.5}\|$ $[Al_{4.9}Si_{13.1}O_{36}]$	2.65 (2.60)	400	360	40
K-Al-offretite(II)	TEA^+, TMA^+	1.41	5.84	2.40	9.65 (10.1)	4.78	$\|TEA_{0.3}TMA_{1.4}Na_{0.1}K_{2.7}OH_{0.3}(H_2O)_{5.2}\|$ $[Al_{4.2}Si_{13.8}O_{36}]$	3.28 (2.93)	470	450	20
Na-Ga-omega	TEA^+, TMA^+	0.97	3.82	2.06	6.85 (5.8)	4.56	$\|TEA_{0.4}TMA_{2.4}Na_{7.2}K_{0.1}OH_{0.3}(H_2O)_{18.8}\|$ $[Ga_{9.9}Si_{26.1}O_{72}]$	2.63 (2.66)	—[d]	—[d]	—[d]
Rb-Al-merlinoite	TEA^+, TMA^+	0.62	2.86	1.73	5.21 (4.0)	5.32	$\|TEA_{0.6}TMA_{1.2}Rb_{7.6}K_{0.2}OH_{0.7}(H_2O)_{17.2}\|$ $[Al_{8.9}Si_{23.1}O_{64}]$	2.61 (2.79)	—[d]	—[d]	—[d]
K-Al-UZM-12	TEA^+, HM^{2+}	2.26	12.11	3.31	17.69 (19.0)	6.19	$\|TEA_{0.3}HM_{2.5}Na_{0.5}K_{2.1}OH_{1.6}(H_2O)_{5.7}\|$ $[Al_{6.3}Si_{29.7}O_{72}]$	4.74 (4.15)	480	460	20
K-Ga-UZM-12	TEA^+, HM^{2+}	1.77	9.32	2.63	13.72 (14.9)	6.10	$\|TEA_{0.1}HM_{2.1}Na_{0.3}K_{2.3}OH_{1.3}(H_2O)_{6.0}\|$ $[Ga_{5.6}Si_{30.4}O_{72}]$	5.39 (4.13)	300	280	20
Li-Al-EU-1	TEA^+, HM^{2+}	1.67	8.67	2.13	12.47 (12.8)	6.03	$\|TEA_{0.1}HM_{4.7}\ Li_{1.6}Na_{0.1}(H_2O)_{9.6}\|$ $[Li_{1.5}Al_{6.7}Si_{103.8}O_{224}]$[e]	15.5	340	240	100
K-Ga-EU-1	TEA^+, HM^{2+}	1.49	7.78	1.96	11.23 (13.1)	6.05	$\|TEA_{0.1}HM_{4.6}Na_{0.2}K_{3.3}OH_{5.6}(H_2O)_{11.5}\|$ $[Ga_{7.2}Si_{104.8}O_{224}]$	14.5	200	150	50
Na-Al-sodalite	Ch^+	2.89	10.07	2.86	15.83 (19.6)	4.03	$\|TMA_{2.0}Na_{0.1}Sr_{0.1}OH_{0.3}(H_2O)_{0.5}\|$ $[Al_{2.0}Si_{10.0}O_{24}]$	4.99 (4.82)	—[d]	—[d]	—[d]
Cs-Ga-sodalite	Ch^+	2.49	8.77	2.44	13.69 (15.4)	4.08	$\|TMA_{1.8}Cs_{0.04}Sr_{0.1}H_{0.1}(H_2O)_{0.8}\|$ $[Ga_{2.3}Si_{9.7}O_{24}]$	4.30 (4.34)	—[d]	—[d]	—[d]
Li-Al-UZM-22	Ch^+	3.10	13.51	3.51	20.12 (24.0)	5.05	$\|Ch_{5.4}Li_{0.1}Sr_{0.3}OH_{0.3}(H_2O)_{6.1}\|$ $[Al_{5.9}Si_{28.1}O_{68}]$	4.76 (2.06)	630	580	50
Rb-Al-UZM-22	Ch^+	2.87	12.44	3.37	18.68 (22.4)	5.01	$\|Ch_{5.4}Rb_{0.4}Sr_{0.7}OH_{0.6}(H_2O)_{8.5}\|$ $[Al_{6.8}Si_{27.3}O_{68}]$	4.04 (1.96)	570	420	150
Cs-Al-UZM-22	Ch^+	2.94	12.76	3.45	19.15 (23.8)	5.03	$\|Ch_{5.5}Cs_{0.1}Sr_{0.6}OH_{0.8}(H_2O)_{7.5}\|$ $[Al_{5.9}Si_{28.1}O_{68}]$	4.75 (1.99)	730	650	80

[a] The total organic contents in wt%. The values given in parentheses are exothermic weight losses by TGA/DTA at 250−800 °C. [b] Determined from a combination of elemental and thermal analyses. The water content was calculated from the endothermic weight loss by TGA/DTA up to 250 °C, and OH^- or H^+ has been introduced to make the as-made zeolites electrically neutral. [c] Me is Al or Ga. The values given in parentheses are the Si/Me ratios calculated from the ^{29}Si MAS NMR spectra. [d] Not determined. [e] The idealized formula in which neither OH^- nor H^+ was introduced for the net charge compensation.

dx.doi.org/10.1021/ja1095057 | J. Am. Chem. Soc. 2011, 133, 1917–1934

Table 2 gives the crystallographic data for a series of aluminosilicate and gallosilicate zeolites described above. Despite the long Ga-O bond (1.83 Å) compared to the Al−O bond (1.75 Å), no significant expansions in the unit cell volume caused by moving the trivalent lattice-substituting component from Al to Ga were observed for all gallosilicate zeolites except K-Ga-UZM-12. This can be rationalized by considering that the unit cell volume is related not only to the T−O bond distances but also to the T−O−T bond angles,[23] which can be further supported by the structural IR data. As seen in Table 2, K-Ga-UZM-12 exhibits the asymmetric T−O stretching band at 1055 cm^{-1} which is lower by 13 cm^{-1} than the band position (1068 cm^{-1}) obtained from K-Al-UZM-12. However, no significant differences in this stretching band position were observed for the other three pairs of aluminosilicate and gallosilicate zeolites. A quite similar trend can also be found in the position for their T−O bending bands.

Table 3 lists the chemical compositions of 16 selected zeolites obtained in our study. When more than one type of organic SDA is used in zeolite syntheses, there is a very high enrichment of organic species used as a crystallization SDA in products compared to that used as a CDM SDA. As seen in Table 3, the TEA^+/TMA^+ ratios (≤0.5) of all five offretite materials are much lower than the ratio (16) of their synthesis mixtures. A similar trend can be observed not only for Na-Ga-omega and Rb-Al-merlinoite obtained in the same TEA^+-TMA^+ mixed-organic system but also for UZM-12 and EU-1 zeolites prepared in the TEA^+-HM^{2+} system. On the other hand, the synthesis of MER-type zeolites in both presence and absence of organic SDAs have long been reported.[24] Camblor and co-workers have successfully synthesized merlinoite with a Si/Al ratio of 3.8 using TEA^+ only as an organic SDA together with K^+.[24d] Despite the addition of both TEA^+ and TMA^+ as organic SDAs to its synthesis mixture, by contrast, the Si/Al ratio (2.6) of our merlinoite was found to be considerably lower than the ratio (4.2) of the same zeolite prepared from a rubidium aluminosilicate synthesis mixture with Si/Al = 4.5 without recourse to organic SDAs.[24f] Table 3 also shows that the C/N ratios (∼4) of both Na-Al-sodalite and Cs-Ga-sodalite are noticeably lower than the ratio (5) of Ch^+ used as an organic SDA in their crystallization, unlike the case of UZM-22 zeolites obtained in the presence of the same organic SDA. Since the longest dimension (7.0 Å) of the free Ch^+ ion calculated using Chem 3D Ultra version 11.0 (CyberChem) is larger than the diameter (6.6 Å) of the β-cages of sodalite materials, we speculate that this organic may be modified in situ under synthesis conditions and then involved in sodalite crystallization. Further evidence to support this speculation will be given below.

It is also remarkable from the chemical composition data in Table 3 that although their synthesis includes no intentional addition of K^+, some zeolites contain a nonnegligible amount of this alkali cation. For example, Na-Ga-offretite(I) and Na-Al-offretite(II) were characterized to have 0.9 and 0.5 K^+ ions per unit cell, respectively. Since the K^+ impurity levels of all reagents used in the synthesis of these zeolites are ca. 50 ppm or lower, their K^+ ions may in our view come from the Teflon liners that had already been used in synthesis experiments. Prior to the reuse, in fact, we routinely cleaned up the used Teflon liners by first immersing them in 5 wt % HF solutions and then in 5 wt % KOH solutions. To check whether the offretite structure can crystallize from a K^+-free gallosilicate synthesis mixture, therefore, we attempted to reproduce the synthesis of Na-Ga-offretite(I) under the optimized conditions using new Teflon liners. No solids were detected even after 28 days of heating at 100 °C. However, replacement of even a quarter the amount of NaCl by KCl in the synthesis mixture followed by 14 days of heating resulted in the formation of gallosilicate offretite. This again shows that the ability of K^+ yielding the offretite structure is much more selective than that of Na^+.

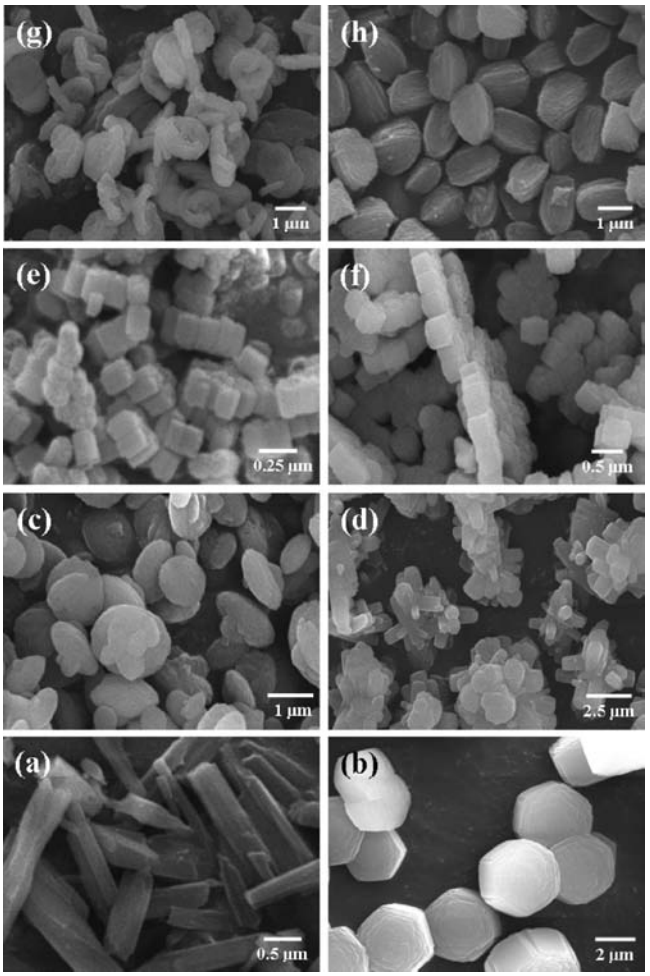

Figure 2. SEM images of as-made (a) K-Ga-offretite(I), (b) Na-Ga-offretite(I), (c) Na-Al-offretite(II), (d) K-Al-offretite(II), (e) K-Ga-offretite(IV), (f) Rb-Ga-offretite(IV), (g) Na-Ga-omega, and (h) Rb-Al-merlinoite.

Figure 2 shows the SEM images of six different offretite materials, together with Na-Ga-omega and Rb-Al-merlinoite, which were prepared under the conditions given in Table 1. K-Ga-offretite(I) appears as needle-like crystals of ca. 2 μm in length, a typical morphology for this zeolite.[25] Of particular interest is the crystal morphology of Na-Ga-offretite(I), characterized by well-faceted, hexagonal plates of approximately 4.0 μm in diameter and 1.0 μm in thickness, hence with an aspect ratio much lower than 1. In addition, Na-Al-offretite(II) and K-Al-offretite(II) consist of round, fat plates of ca. 1 μm in diameter and heavily overlapped hexagonal rods of ca. 2 μm in length, respectively. We should note here that when a small portion (e.g., one-fourth) of the NaCl in the synthesis mixture used for Na-Ga-offretite(I) formation is replaced by KCl, the crystallized product has a quite similar crystal morphology to that of K-Ga-offretite(I). It thus appears that Na^+ and K^+ ions play a

dx.doi.org/10.1021/ja1095057 |J. Am. Chem. Soc. 2011, 133, 1917–1934

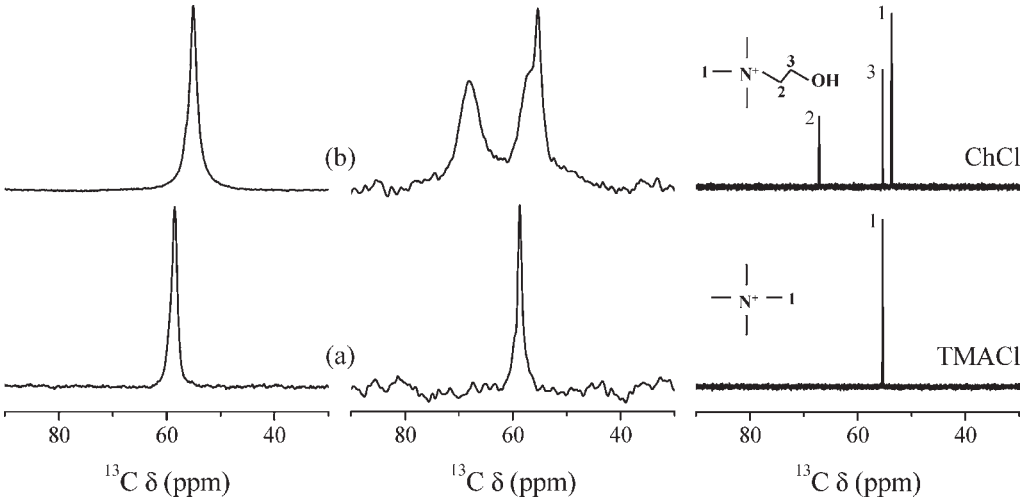

Figure 3. ^{13}C MAS (left) and ^{1}H−^{13}C CP MAS (middle) NMR spectra of as-made (a) Na-Al-sodalite and (b) Li-Al-UZM-22 prepared using choline hydroxide (ChOH) as an organic SDA. The right traces are the ^{13}C NMR spectra in D_2O solution of TMACl and ChCl.

beneficial role in accelerating the rate of offretite crystal growth along the *ab*-plane and *c*-axis, respectively.

Unlike these four offretite zeolites prepared in the TEA^+−TMA^+ mixed-organic SDA system, by contrast, the K-Ga-offretite(IV) and Rb-Ga-offretite(IV) materials synthesized in the Sr^{2+}−Ch^+ inorganic−organic SDA system are composed of highly uniform, short cylinders that are attached to the sides of one another along their *ab*-plane to form 2D cylinder plates. This attachment is more noticeable for Rb-Ga-offretite(IV) than for K-Ga-offretite(IV), although the crystals of the former material have a lower aspect ratio (1 vs 2). Because more than one-third of the attached crystals of both Rb-Ga-offretite(IV) and K-Ga-offretite(IV) were found to remain intact even after sonication in water for 1 h, they appear to be grown in a somewhat overlapped manner to the *ab*-plane. Figure 2 also shows that Na-Ga-omega has round plates of ca. 1 μm in diameter, unlike the needle-like morphology repeatedly reported for this large-pore material.[26] More interestingly, Rb-Al-merlinoite appears as concave, prismatic crystallites of ca. 1.5 μm in length with doubly arched ends, which is unique among the crystal morphologies of MER materials reported thus far.[24] Therefore, it is clear that the crystal morphologies of zeolites prepared here are quite different from those of the corresponding materials crystallized in the already known conditions. We speculate that the rates of zeolite crystal growth along particular axes and/or planes in highly basic CDM synthesis conditions (normally pH > 13) may be significantly different from those in conventional synthesis conditions. The details are, however, beyond the scope of our study.

The ^{13}C MAS NMR spectra of the representative zeolites obtained from four different mixed-SDA systems described above can be found in Supporting Information Figure S2 . These data reveal that organic SDAs used in their synthesis end up entrapped within their pores. In fact, all organic species used in zeolite syntheses performed here were found to remain intact upon their entrapment into the void spaces of zeolitic products, with the exception of Ch^+ leading to the crystallization of sodalite materials in the presence of Sr^{2+} and some alkali cations at 150 °C (Table 1). The ^{13}C MAS NMR data in Supporting Information Figure S2 also show that the resonances from TEA^+ used as a CDM SDA in the presence of TMA^+ or HM^{2+} are barely detectable for all zeolites crystallized, which is consistent with the chemical composition data in Table 3.

Figure 3 shows the ^{13}C MAS and ^{1}H−^{13}C CP MAS NMR spectra of as-made Na-Al-sodalite and Li-Al-UZM-22 synthesized in the Sr^{2+}−Ch^+ SDA system. For comparison, the liquid ^{13}C NMR spectra in D_2O solutions of ChCl and TMACl are also given in Figure 3. Only one resonance around 58 ppm was found in both ^{13}C MAS and ^{1}H−^{13}C CP MAS NMR spectra of as-made Na−Al-sodalite, which is also the case of the other sodalites obtained in this study. As described above, the Ch^+ ion is too big to be encapsulated within the β-cages of sodalite materials without experiencing severe geometric constraints. Furthermore, this OH group-containing cation is reported to decompose into TMA^+ at 135 °C or so[27] which is lower than the crystallization temperature (150 °C) of our sodalites. Since the ^{13}C resonance from Na-Al-sodalite has nearly the same chemical shift as the values observed for TMA^+ in SOD materials with different framework compositions,[28] it is clear that the encapsulated species in Na-Al-sodalite is not Ch^+ but TMA^+, which is a new example of in situ organic SDA modification under zeolite synthesis conditions.[27,29] Another interesting result obtained from Figure 3 is that while the ^{1}H−^{13}C CP MAS NMR spectrum of as-made Li-Al-UZM-22 is characterized by three resonances around 55, 57, and 68 ppm, its ^{13}C MAS NMR spectrum gives only one resonance around 55 ppm, unlike the case of K-Al-offretite(IV) or K-Ga-offretite(IV) prepared using the same organic SDA (Supporting Information Figure S2). The same result was also observed for the other three UZM-22 zeolites prepared here. Therefore, it is most likely that Ch^+ remains intact upon occlusion into the UZM-22 pores, but the spatial constraints imposed on two different CH_2 carbons of the organic guest molecule are much more severe than those on its CH_3 carbons, hence making the former carbons much less mobile.

Figure 4 shows the IR spectra of as-made Li-Al-UZM-22 in the 2500 − 4000 cm^{-1} recorded at different temperatures, together with the room-temperature IR spectrum of ChCl. Prior to IR experiments, as described above, the self-supporting pellet of as-made Li-Al-UZM-22, as well as the KBr pellet containing ChCl, was heated under vacuum to a residual pressure of 10^{-3} Torr overnight at 200 °C to completely remove water in the pellet.

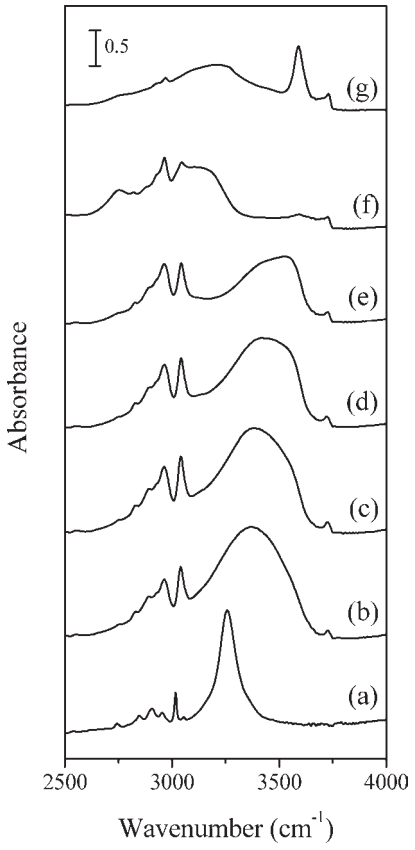

Figure 4. IR spectra in the 2500−4000 cm^{-1} region of (a) ChCl recorded at room temperature and (b−g) as-made Li-Al-UZM-22 recorded at different temperatures: from b to g: 25, 100, 200, 300, 400, and 500 °C.

The IR spectra (not shown) of the dried pellets in the 1500 − 2500 cm^{-1} region gave no detectable bands around 1640 cm^{-1} due to bending vibration of water. Therefore, the band appearing in the OH region of the spectra in Figure 4 cannot be from water in ChCl or as-made Li-Al-UZM-22. The O−H stretching region of ChCl is characterized by a broad and strong band around 3258 cm^{-1} due to its OH group, the proton of which is involved in hydrogen bonding to the Cl^- ion (i.e., O−H···Cl^- hydrogen bonding).[30] As seen in Figure 4, however, the room-temperature IR spectrum of as-made Li-Al-UZM-22 shows a strong but much broader band around 3370 cm^{-1}. Since the position of this band is higher by ca. 110 cm^{-1} than that (3258 cm^{-1}) of the hydrogen-bonded OH band observed for the IR spectrum of ChCl, we can rule out the possibility that the broad band appearing around 3370 cm^{-1} could be due to the O−H···Cl^- hydrogen bonding, although Li-Al-UZM-22 was synthesized using LiCl as a Li^+ source. Therefore, the alternative way to rationalize its occurrence can be achieved by considering the intermolecular hydrogen bonding (i) between two Ch^+ ions within the 12-ring channels of Li-Al-UZM-22 and (ii) to the zeolite framework, and (iii) the intramolecular hydrogen bonding between the oxygen of the OH group of the occluded Ch^+ ion and the protons of the CH_3 carbons linked to its charged nitrogen (i.e., intramolecular C−H···O hydrogen bonding).[30c]

In principle, the formation of two different types of intermolecular hydrogen bonds between Ch^+ ions is possible: one formed between their OH groups and the other between the oxygen of the OH group of the first molecule and the protons of CH_3 carbons linked to the charged nitrogen of the second molecule (i.e., intermolecular C−H···O hydrogen bonding). If the organic SDA molecule in as-made Li-Al-UZM-22 has either of these two conformations, no significant differences in the mobility of their carbon atoms should then be observed. As seen in Figure 3, however, this is not the case. Also, the guest molecule involved in intermolecular hydrogen bonding to the zeolite framework oxygens in AlO_4^- tetrahedra cannot be a correct answer, because the negative framework charge created by Al substitution would rather be balanced by the positively charged nitrogen of the Ch^+ ion than be involved in hydrogen bonding to its OH group. These arguments taken in total lead us to attribute the strong band appearing around 3370 cm^{-1} in the IR spectrum of as-made Li-Al-UZM-22 to the OH group of the occluded Ch^+ ion involved in intramolecular C−H···O hydrogen bonding. Thus, if only the rotation with respect to the C−C bond in the 2-hydroxyethyl chain is considered, the mobility of CH_2 carbons in such a gauche conformer should be considerably lower than that of its CH_3 carbons (Figure 3). This can be rationalized when the strength of intramolecular C−H···O hydrogen bonding in Ch^+ cannot be strong enough to cause a notable shift of the C−H stretching vibration of its CH_3 groups. As seen in Figure 4, in fact, the position (3041 cm^{-1}) of the CH_3 C−H stretching band from as-made Li-Al-UZM-22 is considerably higher than that (3016 cm^{-1}) from ChCl, the CH_3 proton of which is involved in hydrogen bonding to the Cl^- ion (i.e., C−H···Cl^- hydrogen bonding).[30c] Furthermore, there are no noticeable changes in the C−H stretching band position for as-made Li-Al-UZM-22, although the IR spectra were taken at 300 °C or even higher, suggesting the weak nature of intramolecular C−H···O hydrogen bonding in the organic SDA occluded. To our knowledge, the Ch^+ ion in UZM-22 is the first example where this type of intramolecular hydrogen bond can be formed within the organic SDA molecules in as-made zeolites.

Figure 4 also shows that the general feature of the IR spectrum of as-made Li-Al-UZM-22 remains almost unchanged at 100 °C. Therefore, it is clear that the intramolecular C−H···O hydrogen bond in the occluded Ch^+ ion is preserved even at the crystallization temperature of the zeolite host. This suggests that the gauche conformer of Ch^+ with one intramolecular C−H···O hydrogen bond may play a role during nucleation at the crystallization temperature (100 °C) in the lithium aluminosilicate synthesis mixture. Prior to our work on the Ch^+ ion in UZM-22, the ethylene glycol occluded in (alumino)silicate sodalite and the cobaltocenium ($Co(C_5H_5)_2^+$) ion in all-silica nonasil (NON) were only two cases in which the preservation of hydrogen bonds within organic SDA molecules or between the organic SDA molecule and the zeolite framework at the crystallization temperature of the host has been clearly established.[31] With increasing the treatment temperature to 300 °C, on the other hand, the O−H stretching band around 3370 cm^{-1} in the IR spectrum of as-made Li-Al-UZM-22 becomes weaker and one broad band around 3550 cm^{-1} assignable to the free OH group of Ch^+ appears. A further increase of treatment temperature to 400 °C or higher resulted in the disappearance of the two broad bands around 3370 and 3550 cm^{-1} accompanied by the appearance of a rather sharp band at 3591 cm^{-1} due to acidic bridging OH groups of the Brønsted acid sites,[32] which must be a result of the

dx.doi.org/10.1021/ja1095057 |J. Am. Chem. Soc. 2011, 133, 1917–1934

decomposition of the occluded organic SDA as can be confirmed by the TGA/DTA curves for as-made Li-Al-UZM-22 in Supporting Information Figure S3. It thus appears that the intramolecular C−H···O hydrogen bond in Ch^+ breaks prior to the organic SDA decomposition.

Figure 5 shows the ^{1}H MAS NMR spectra of the as-made and proton forms of Li-Al-UZM-22. For comparison, the liquid ^{1}H NMR spectrum in D_2O solution of ChCl is also given in Figure 5. ChCl exhibits four ^{1}H resonances at 3.34, 3.66, 4.17, and 4.80 ppm. The first three lines are due to the CH_3 protons and the CH_2 protons linked to nitrogen and oxygen, respectively. It is worthwhile to note that the chemical shift of the OH proton involved in hydrogen bonding to the Cl^- ion varies with the strength of hydrogen bonding: for example, the OH proton subject to extensive hydrogen bonding appears at a fairly low field (5.22 ppm).[30b] Therefore, the line at 4.80 ppm in the liquid ^{1}H NMR spectrum of ChCl can be assigned to the combination of the labile OH proton of Ch^+ and the water in D_2O. As seen in Figure 5b, on the other hand, the ^{1}H MAS NMR spectrum of as-made Li-Al-UZM-22 is characterized by a very broad and weak line around 5 ppm and a weak line at 4.4 ppm, as well as by a very strong line at 3.4 ppm. The high-field line can be attributed to the combination of the free CH_3 protons and the CH_3 protons forming a weak, intramolecular hydrogen bond to the OH group of the organic SDA molecule, because the mutual exchange of the free and hydrogen-bonded CH_3 groups of the occluded Ch^+ ion in Li-Al-UZM-22 could be very fast with the NMR time scale. Also, the broad line around 5 ppm is mainly due to water.[23b] Interestingly, deconvolution of the ^{1}H MAS NMR spectrum of as-made Li-Al-UZM-22 reveals that the two lines around 4.4 and 3.4 ppm have an intensity ratio of approximately 1:13 which is the same as the number ratio (1:13) between the OH proton of Ch^+ and its CH_3 and CH_2 protons. The slight high-field shift (4.4 vs 4.8 ppm) of the weak OH line in comparison to ChCl subject to hydrogen bonding to Cl^- is consistent with the IR evidence for the presence of intramolecular C−H···O hydrogen bonding within the Ch^+ ions occluded in Li-Al-UZM-22.

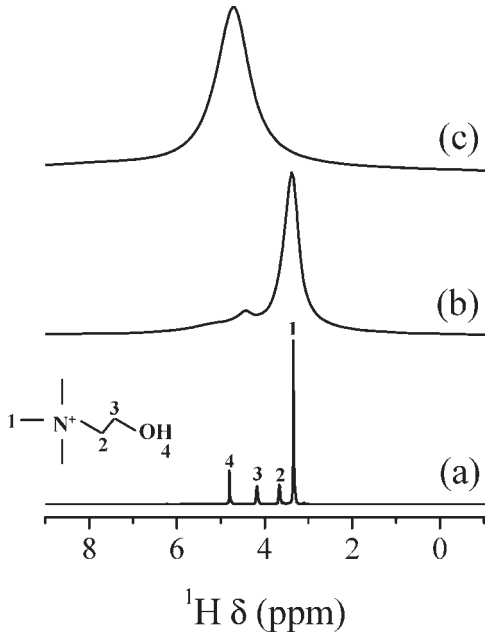

Figure 5. (a) ^{1}H NMR spectrum in D_2O solution of ChCl, showing the assignment of each resonance, and ^{1}H MAS NMR spectra of the (b) as-made and (c) proton forms of Li-Al-UZM-22.

^{27}Al MAS NMR measurements on as-made aluminosilicate zeolites synthesized in our study reveal that all of them, except Li-Al-EU-1 obtained from the TEA^+−HM^{2+} double-organic additive system, give only one ^{27}Al resonance at 50−60 ppm, typical of tetrahedral Al sites.[33] In addition, the presence of Ga in the tetrahedral framework positions of all as-made gallosilicate zeolites obtained here can be evidenced by the fact that their ^{71}Ga MAS NMR spectra are always characterized by one broad line at 150−170 ppm.[7,18,33] The ^{29}Si MAS NMR spectra of as-made K-Al-UZM-12 and K-Ga-UZM-12, together with the simulated spectra and their deconvoluted components, can be found in Supporting Information Figure S4. We note here that the number of deconvoluted components is higher for the spectrum of the gallosilicate analogue of this ERI-type material than for its aluminosilicate counterpart, like the case of OFF-type zeolites.[34] It is well-established that zeolite framework Si atoms become more deshielded upon isomorphous substitution of Al by

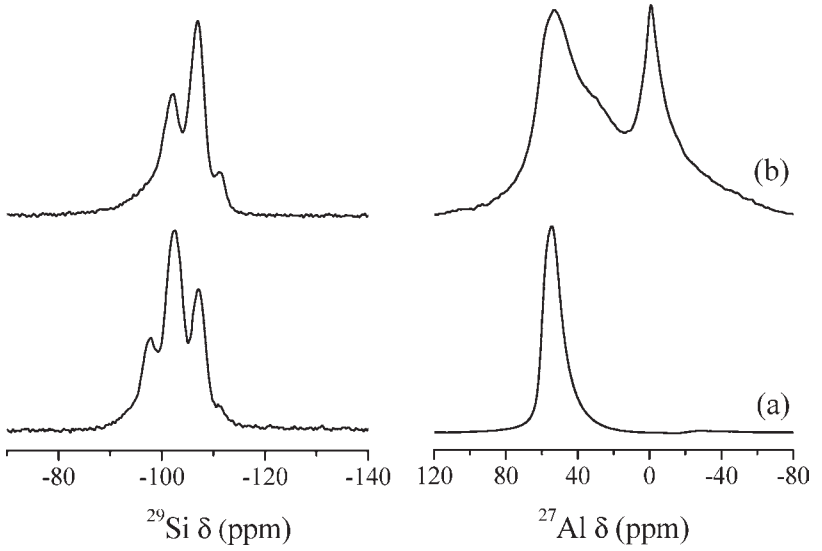

Figure 6. ^{29}Si (left) and ^{27}Al (right) MAS NMR spectra of the (a) as-made and (b) proton forms of Li-Al-UZM-22.

Table 4. Experimental and Predicted ^{27}Al NMR Chemical Shifts of ZSM-18 and UZM-22

		ZSM-18					UZM-22				
Al site	multiplicity	average ∠T-O-T[a]	^{27}Al δ, ppm from $Al(H_2O)_6^{3+}$ δ_{pre}[b]		δ_{obs}[c]	Δδ[d]	average ∠T-O-T[e]	^{27}Al δ, ppm from $Al(H_2O)_6^{3+}$ δ_{pre}[b]		δ_{obs}[f]	Δδ[d]
Al1	4	163.5	45.6	(11.8)	53.9 (41.2)	8.3	159.3	48.6	(11.8)	45.3 (13.7)	-3.3
Al2	12	147.3	57.3				142.0	61.2			
Al3	12	148.0	56.8	(88.2)	59.6 (58.8)	1.8	143.7	59.9	(88.2)	54.5 (86.3)	-6.1
Al4	6	142.5	60.8				142.5	60.8			

[a] Average T−O−T angles in degrees from the crystallographic data for H-ZSM-18 reported by Lawton and Rohrbaugh.[35] [b] Predicted chemical shifts from the average T−O−T angles using the equation of Jacobsen et al.[37] The values given in parentheses are the ideal relative intensities calculated from the multiplicity of four crystallographically different T-sites in MEI framework. [c] Observed chemical shifts (from the two-component deconvolution of the experimental spectrum for NH_4-ZSM-18 in ref 36) with their relative intensities given in parentheses. [d] $\Delta\delta = \delta_{obs} - \delta_{pre}$, difference between observed and predicted chemical shifts. The average δ_{pre} (57.8 or 60.6 ppm) for sites Al2, Al3, and Al4 in H-ZSM-18 or as-made UZM-22 was calculated based on their multiplicities. [e] Average T−O−T angles in degrees from the crystallographic data for as-made Li-Al-UZM-22 reported by Wang et al.[17] [f] Observed chemical shifts (from the two-component deconvolution of the experimental spectrum for as-made Li-Al-UZM-22 in Figure 6) with their relative intensities given in parentheses.

Ga.[23c,33] Thus, if two or more crystallographically different T-sites exist in a particular structure type of zeolites, comparing the ^{29}Si MAS NMR spectra of its gallosilicate and aluminosilicate analogues could be useful for proving their existence.

Figure 6 shows the ^{29}Si and ^{27}Al MAS NMR spectra of the as-made and proton forms of Li-Al-UZM-22 with the MEI topology consisting of 12-ring (6.9 × 6.9 Å) channels along the *c*-axis intersected by 7-ring (3.2 × 3.5 Å) openings.[19,35] Five resonances around −111, −107, −102, −98, and −94 ppm can be distinguished from the ^{29}Si MAS NMR spectrum of as-made Li-Al-UZM-22, the line shape of which is quite similar to that recently reported.[17] Attempts to deconvolute this spectrum by assuming each of the four Si[*n*Al,(4-*n*)Si] lines with $n = 0-4$ as a single Si environment gave a $(Si/Al)_{NMR}$ ratio of 2.06. Since this value is considerably lower than that (4.76) obtained from elemental analysis (Table 3), it appears that the T−O−T angle range for the four crystallographically different T-sites of the Li-Al-UZM-22 framework is not narrow enough to get into a single ^{29}Si line envelope. Figure 6 also shows that conversion of as-made Li-Al-UZM-22 into its proton form results in significant spectral changes, which is indicative of severe dealumination. Unlike the ^{27}Al MAS NMR spectrum of its as-made form, in fact, the ^{27}Al MAS NMR spectrum of the proton form of Li-Al-UZM-22 shows a strong line around 0 ppm and a shoulder around 30 ppm assigned to octahedral and penta-coordinated Al species, respectively.[33] Considering that its N_2 BET surface area is higher than 600 $m^2\ g^{-1}$ (Table 3), however, Li-Al-UZM-22 appears to maintain the overall structural integrity even after conversion into the proton form.

Another interesting observation obtained from Figure 6 is that unlike the spectrum of the ammonium form of its framework type material (i.e., NH_4-ZSM-18), in which two ^{27}Al resonances are reported to be clearly visible,[36] the ^{27}Al MAS NMR spectrum of as-made Li-Al-UZM-22 exhibits only one slightly asymmetric signal around 55 ppm. A quite similar line shape was also observed for the other three UZM-22 zeolites prepared using Na^+, Rb^+, or Cs^+, instead of Li^+. Table 4 lists the ^{27}Al MAS NMR chemical shifts of Al(4Si) species over four different T-sites in this MEI-type zeolite calculated using the equation of Jacobsen et al.[37] and the reported average T−O−T angles for each T-site in as-made UZM-22.[17] The chemical shifts of Al(4Si) species over each T-site in NH_4-ZSM-18 have also been calculated in the same manner as that described above and are listed in Table 4. Despite both the empirical nature of the relationship used in calculating the chemical shifts and the possible inaccuracy of the average T−O−T angles employed,[35−37] a reasonable match between the predicted ^{27}Al chemical shifts and the experimental values is observed for both NH_4-ZSM-18 and as-made Li-Al-UZM-22. This suggests that the assignments of their ^{27}Al resonances to the specific structural units listed in Table 4 are reliable, which may also be the case of their relative intensities. We should note here that the relative intensity (13.7 vs 41.2%) of the high-field component assigned to site Al1 is much smaller for as-made Li-Al-UZM-22 than for NH_4-ZSM-18 but is similar to the relative intensity (11.8%) calculated from the site multiplicity. Therefore, it is clear that unlike ZSM-18, Li-Al-UZM-22 has no significant preference of Al substitution for a particular T-site, which can be further supported by the 2D ^{27}Al Multiplex SPAM 3Q MAS NMR data. As can be found in Supporting Information Figure S5, deconvolution of the ^{27}Al 3Q MAS isotropic projection spectrum of as-made Li-Al-UZM-22 indicates three contributions around 66, 59, and 54 ppm with relative intensities of 30:59:11 assignable to sites Al4, Al3 + Al2, and Al1, respectively. While the Al distribution over site T1 in Li-Al-UZM-22 is approximately one-fourth of the value (41.2%) found in NH_4-ZSM-18, it is again almost identical to the statistical population (11.8%) of site T1 (Table 4).

Figure 7 compares the lowest-energy conformations for the rigid aromatic triquaternary ion 2,3,4,5,6,7,8,9-octahydro-2,2,5,5,8,8-hexamethyl-1*H*-benzo[1,2-*c*:3,4-*c*′:5,6-*c*″]tripyrrolium (HMBTP) and the flexible aliphatic triquaternary ion tris-(2-trimethylammonioethyl)amine (TMAEA) used initially and subsequently to synthesize ZSM-18, respectively, with those for the flexible monoquaternary ions triethanolmethylammonium (TEMA) and Ch^+ used to crystallize ECR-40, the silicoaluminophosphate analogue of ZSM-18, and UZM-22, respectively.[2c,36,38] The gauche conformation for the Ch^+ ion stabilized by one intramolecular hydrogen bond between the oxygen of its OH group and the protons of carbon linked to charged nitrogen is also compared in Figure 7. Previous molecular modeling studies predicted a nearly perfect fit of HMBTP with the longest dimension of 10.3 Å into the 12-ring channel of ZSM-18 with the same 3-fold rotational symmetry as that of the rigid organic molecule.[39] In fact, the guest−host interactions in as-made ZSM-18 were found to be sufficient to strictly limit rotations of the occluded triquaternary ion.[40] Since rotations about axes of symmetry are commonly observed for other organic SDAs entrapped inside zeolitic void spaces, therefore,

dx.doi.org/10.1021/ja1095057 |*J. Am. Chem. Soc.* 2011, 133, 1917–1934

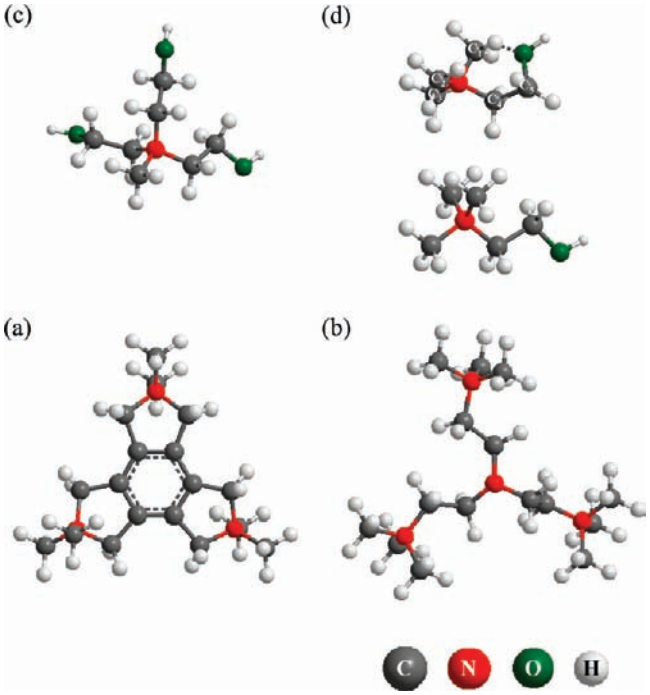

Figure 7. Contrast between the lowest-energy conformations for the triquaternary cations (a) 2,3,4,5,6,7,8,9-octahydro-2,2,5,5,8,8-hexamethyl-1*H*-benzo[1,2-*c*:3,4-*c*′:5,6-*c*″]tripyrrolium, (b) tris(2-trimethylammonioethyl)amine, both of which were used to synthesize ZSM-18, and those for the monoquaternary cations (c) triethanolmethylammonium and (d) choline that were used to crystallize, ECR-40, the silicoaluminophosphate analogue of ZSM-18, and UZM-22, respectively. The gauche conformation for choline stabilized by one intramolecular C−H···O hydrogen bond is also given in panel d.

HMBTP in the synthesis of ZSM-18 has long been considered as a prime example of true templating. If such were the case, the nitrogen atoms in its 5-rings should have a direct spatial association with the framework Al atoms in close proximity of the 7-ring-opening normal to the 12-ring channel for charge compensation. This does not mean that Al is ordered into particular T-sites in as-made ZSM-18. However, it is not very difficult to speculate that the spatial arrangement of trivalent framework atoms can differ according to the rigidity of the organic SDA employed, as well as to its charge distribution. Although energy minimization calculations reveal that the longest dimension (11.0 Å) of the free TMAEA ion is slightly longer than that (10.3 Å) of the free HMBTP ion, on the other hand, the degree of nonrandom Al distribution over the four different T-sites in ZSM-18 synthesized using the former SDA could be lower than that in the same material prepared with the latter one. This is because the aliphatic TMAEA molecule has a much higher degree of flexibility. Such a less nonrandom nature of Al distribution should be more apparent to the UZM-22 zeolite crystallized using the smaller Ch^+ ion, especially when the cation ends up encapsulated with one intramolecular C−H···O hydrogen bond (Figures 3−5), hence having the longest dimension (5.8 Å) shorter by ca. 1 Å than that (7.0 Å) of the free molecule. In other words, the Ch^+ ion, considerably smaller and much more flexible than HMBTP, has no particular reason for locating framework Al atoms near the 7-ring channel of the MEI structure, explaining why the low-field ^{27}Al resonance from as-made Li-Al-UZM-22 is much weaker than that from

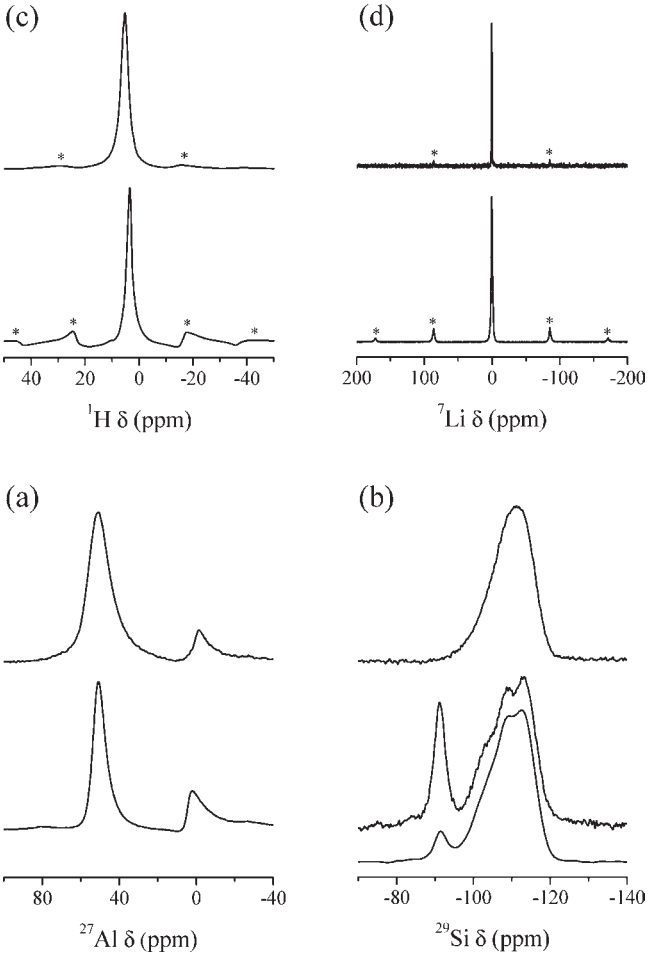

Figure 8. (a) ^{27}Al, (b) ^{29}Si, (c) ^{1}H, and (d) ^{7}Li MAS NMR spectra of the as-made (bottom) and proton (top) forms of Li-Al-EU-1 prepared in the TEA^+−HM^{2+} mixed-organic system. The trace given below the ^{29}Si MAS NMR spectrum of as-made Li-Al-EU-1 is its ^{1}H−^{29}Si CP MAS NMR spectrum. Spinning side bands are marked by asterisks.

NH_4-ZSM-18 (Table 4). Therefore, it appears that the spatial arrangement of Al atoms in the zeolite framework can be tailored by selecting organic SDAs with appropriate sizes and charge distributions, as previously suggested by Lobo and co-workers.[41]

Figure 8 shows the ^{27}Al, ^{29}Si, ^{1}H, and ^{7}Li MAS NMR spectra of the as-made and proton forms of Li-Al-EU-1 zeolite prepared using Li^+ as an inorganic crystallization SDA in the TEA^+−HM^{2+} double-organic additive system. Unlike the spectra of the other zeolites prepared here, the ^{27}Al MAS NMR spectrum of as-made Li-Al-EU-1 exhibits an additional weak ^{27}Al resonance around 0 ppm assigned to octahedral Al, as well as a much stronger line around 51 ppm. Although the period of crystallization time at 150 °C increased from 14 to 28 days, the resulting Li-Al-EU-1 zeolite still showed a weak ^{27}Al resonance around 0 ppm (Supporting Information Figure S6). It thus appears that this octahedral Al line is not due to the imperfect crystalline nature of Li-Al-EU-1 but due to the trace amount of extraframework Al species entrapped inside the large EU-1 cavities. Another possible explanation is the existence of a small amount of a layered phase containing octahedral Al species in Li-Al-EU-1, because of the presence of a very weak but non-negligible X-ray peak appears around 6.5° in its powder XRD pattern (Figure 1e). In fact, the XRD pattern (not shown) of a

layered phase present as a major impurity in Li-Al-sodalite gave a strong band at this low 2θ angle. Figure 8 also shows that the ^{27}Al MAS NMR spectrum of the proton form of Li-Al-EU-1 shows no detectable increase in relative intensity of the octahedral signal, suggesting the high thermal stability of its framework Al atoms.

The most interesting but unexpected result obtained from Figure 8 is that the ^{29}Si MAS NMR spectrum of as-made Li-Al-EU-1 is characterized by one strong and symmetric ^{29}Si resonance at −91.3 ppm, as well as by three less resolved lines around −103, −108, and −114 ppm assigned to crystallographically different Q^4 units[33,42] (Q^n represents $(SiO)_nSiX_{4-n}$, where X is OH or O^-). Neither as-made Na-Al-EU-1, a conventional aluminosilicate EU-1 with Si/Al = 26 prepared using Na^+ and HM^{2+} as SDAs,[8] nor as-made K-Ga-EU-1 was found to give such a strong ^{29}Si resonance around −90 ppm (Supporting Information Figure S7). Also, no notable increase in relative intensity of this low-field ^{29}Si resonance was detected even after a longer period (28 days) of heating at 150 °C (Supporting Information Figure S6). Given its chemical shift, the ^{29}Si resonance at −91.3 ppm could be simply attributed to $(SiO)_2Si(OH)_2$ groups (i.e., Q^2 defect sites) rather than to SiO^-Li^+, SiO^-R^+, where R^+ is the ammonium moiety of organic SDAs (mainly HM^{2+}; see Table 3), or SiOH groups (i.e., Q^3 defect sites).[33,42] As seen in Figure 8, however, the ^{1}H MAS NMR spectrum of as-made Li-Al-EU-1 exhibits only one line at 3.5 ppm due to the protons of organic SDAs. The lack of any noticeable ^{1}H resonance in the chemical shift region 10−20 ppm suggests the actual absence of SiOH groups involved in strong hydrogen bonding with neighboring SiO^- groups (i.e., $SiOH\cdots SiO^-$ hydrogen-bonded hydroxyls).[39a,43] Because the relative intensity of the ^{29}Si resonance around −91 ppm was found to be much weaker in the ^{1}H−^{29}Si CP MAS NMR spectrum of as-made Li-Al-EU-1 than in its MAS spectrum, in particular, it is clear that the strong ^{29}Si resonance appearing at −91.3 ppm in the ^{29}Si MAS NMR spectrum of as-made Li-Al-EU-1 cannot be attributed to framework defects in this cage-based, medium-pore zeolite, but must be ascribed to its Li^+ ions added as an inorganic crystallization SDA, some of which have been introduced into the EU-1 framework during synthesis.[4a,4b,44]

Deconvolution of the ^{29}Si MAS NMR spectrum of as-made Li-Al-EU-1 indicates that the ^{29}Si resonance at −91.3 ppm has a full width at half-maximum (fwhm) of 210 Hz which is barely half the value (410 Hz) of the ^{29}Si resonance at −114 ppm due to Q^4(4Si). Therefore, we suspect that the distribution of Li atoms over the 10 different T-sites in Li-Al-EU-1 could be nonrandom. We also note that this low-field resonance stands for approximately 20% of the total integrated intensity. Because the idealized unit cell composition of as-made Li-Al-EU-1 (Table 3), to make it electrically neutral, shows that only 1.5 Li atoms (about half the Li content) per unit cell (112 T-atoms) are present in the tetrahedral framework positions; however, the ^{29}Si resonance at −91.3 ppm may in our view be attributed to Q^4(1Li,1Al,2Si) sites rather than to Q^4(1Li,3Si) ones.[4b] Clearly, the introduction of monovalent component like Li into silica frameworks generates the highest framework negative charge of 3− per substitution, rendering the resulting materials most attractive as new ion-exchangers, separation media, and catalysts. Unlike that of as-made Li-Al-EU-1, however, the ^{29}Si MAS NMR spectrum of its proton form gives no detectable lines around −90 ppm (Figure 8). This indicates that the framework Li atoms in Li-Al-EU-1 are not thermally stable.

The ^{7}Li MAS NMR spectrum of as-made Li-Al-EU-1 shows only one narrow line around 0 ppm, together with well developed spinning side bands, which has been repeatedly reported for several lithosilicate zolites with different framework structures.[4b,44] This indicates a strongly anisotropic and fixed local environment for the Li^+ cations, although ^{7}Li MAS NMR spectroscopy is not useful for discriminating between the framework Li atoms and extraframework Li^+ cations. When converted to its proton form, however, the spinning side pattern and central isotropic signal become much less pronounced and stronger, respectively, suggesting the generation of a more asymmetric and possibly motionally averaged environment.

To gain further evidence for the Li substitution in as-made Li-Al-EU-1, we have determined its crystal structure using synchrotron powder diffraction and Rietveld analyses. During the course of the Rietveld refinement, geometric constraints were imposed on the framework and organic SDA molecule (i.e., HM^{2+}) atomic bonding parameters: d_{Si-O} = 1.61(5), d_{O-O} = 2.63(5), d_{C-C} = 1.54(5), and d_{C-N} = 1.47(5) Å. H atoms of the HM^{2+} cation were not included in the refinement. The soft constraints for the framework and organic SDA were initially used with the weighting factor of 20. However, the weighting for the framework was progressively reduced to zero as the refinement converged, while the weighting factor for the organic SDA was decreased to 2 in the final refinement. Simultaneously, the scale for the refinement was determined preliminarily using the data in the high 2θ angle range and set subsequently to the fixed value until the other structural parameters were refined. This is because the contribution of the zeolite framework structure to the high 2θ range was large, but because the extraframework species like organic SDAs affected the low 2θ range more significantly. In order to perform the global optimization, the host zeolite lattice was held rigid during the refinement. However, the HM^{2+} cation occluded was automatically restrained via the dynamic occupancy correction,[13b] allowing the organic SDA molecule to be mobile within the void spaces defined by the zeolite structure. The range of the global optimization was set to 0.4 $\sin(\theta)/\lambda$.[13b] As the refinement proceeded, the scale factor was fitted again. The fitting of the occupancy of HM^{2+} improved the fitting quality for both Na-Al-EU-1 and Li-Al-EU-1. The refined numbers of HM^{2+} molecules per unit cell were 4.5 and 3.5 for Na-Al-EU-1 and Li-Al-EU-1, respectively, which are in a good agreement with the values (4.6 and 4.7, respectively) determined by elemental analysis (Supporting Information Table S1).

Our attempts to locate Li^+ ions at 10 crystallographically different T-sites in as-made Li-Al-EU-1 throughout the Rietveld refinements of framework atom positions were not successful, mainly due to their poor scattering power. Although only 1.5 Li atoms per unit cell with 112 T-atoms were estimated to locate in the tetrahedral framework positions from elemental analysis (Table 3); however, the powder charge-flipping (pCF) analysis[45] of reflection intensities revealed the possibility that framework defects could be located at site T8 or T9. Very recently, the pCF algorithm has been successfully used to prove the nonrandom distribution of B atoms in one of the four crystallographically different T-sites in the novel medium-pore borosilicate zeolite MCM-70 (MVY) with Si/B = 5.[46] Once the possible defect sites had been refined, therefore, the Si occupancies together with HM^{2+} positions were also allowed to vary in order to prove the statistical validity. An acceptable final R_{wp} value of 9.41% for as-made Li-Al-EU-1 was obtained. The final unit cell parameters

Table 5. Final Atomic Coordinates and Displacement and Population Parameters for As-Made Li-Al-EU-1

atom	*x*	*y*	*z*	occupancy	U_{iso}, $10^2 \times Å^2$	multiplicity
Si1	0.2788(5)	0.43342(29)	0.43762(33)	1.0000	1.784(25)	16
Si2	0.1929(5)	0.38060(26)	0.07298(36)	1.0000	1.784(25)	16
Si3	0.2808(4)	0.43604(29)	0.19545(42)	1.0000	1.784(25)	16
Si4	0.1908(4)	0.37058(26)	0.30901(44)	1.0000	1.784(25)	16
Si5	0.0000	0.55496(41)	0.68837(66)	1.0000	1.784(25)	8
Si6	0.0000	0.46381(46)	0.58142(51)	1.0000	1.784(25)	8
Si7	0.0000	0.53914(44)	0.93948(53)	1.0000	1.784(25)	8
Si8	0.0000	0.47212(41)	0.79385(53)	1.0000	1.784(25)	8
Si9	0.6051(11)	0.2500	0.88308(72)	0.583(9)	1.784(25)	8
Si10	0.6258(7)	0.2500	0.73914(45)	1.0000	1.784(25)	8
O1	0.2500	0.1255(8)	0.5000	1.0000	5.02(8)	8
O2	0.2648(10)	0.3874(5)	0.3610(8)	1.0000	5.02(8)	16
O3	0.4011(8)	0.4204(6)	0.4394(8)	1.0000	5.02(8)	16
O4	0.2500	0.0000	0.4054(11)	1.0000	5.02(8)	8
O5	0.2500	0.1374(8)	0.0000	1.0000	5.02(8)	8
O6	0.1697(8)	0.3032(5)	0.0799(7)	1.0000	5.02(8)	16
O7	0.0914(8)	0.3988(5)	0.0675(7)	1.0000	5.02(8)	16
O8	0.2614(11)	0.4083(6)	0.1265(8)	1.0000	5.02(8)	16
O9	0.4129(8)	0.4318(6)	0.2159(6)	1.0000	5.02(8)	16
O10	0.2500	0.0000	0.1955(12)	1.0000	5.02(8)	8
O11	0.2608(19)	0.3815(11)	0.2364(16)	0.498(21)	5.02(8)	16
O12	0.1809(8)	0.3035(5)	0.2785(6)	1.0000	5.02(8)	16
O13	0.1179(8)	0.4088(5)	0.3007(8)	1.0000	5.02(8)	16
O14	0.0001	0.4642(8)	0.2167(9)	1.0000	5.02(8)	8
O15	0.0000	0.5179(9)	0.6201(10)	1.0000	5.02(8)	8
O16	0.0000	0.0000	0.5000	1.0000	5.02(8)	4
O17	0.0000	0.5123(10)	0.8909(10)	1.0000	5.02(8)	8
O18	0.0000	0.0000	0.0000	1.0000	5.02(8)	4
O19	0.6334(12)	0.2500	0.8002(10)	1.0000	5.02(8)	8
O20	0.0000	0.2500	0.0861(15)	1.0000	5.02(8)	4
O21	0.0000	0.2500	0.2833(13)	1.0000	5.02(8)	4
O22	0.2443(20)	0.4047(13)	0.2624(17)	0.502(21)	5.02(8)	16
N13	0.0000	0.2500	0.85679(29)	0.585(2)	6.2(5)	4
N14	0.9101(4)	0.2500	0.46359(29)	0.585(2)	6.2(5)	8
C1	0.9083(4)	0.2500	0.53909(29)	0.585(2)	6.2(5)	8
C2	0.3954(4)	0.28345(30)	0.40489(29)	0.585(2)	6.2(5)	16
C3	0.4662(4)	0.27635(30)	0.34699(29)	0.585(2)	6.2(5)	16
C4	0.0000	0.15956(30)	0.68719(29)	0.585(2)	6.2(5)	8
C5	0.0000	0.16875(30)	0.76289(29)	0.585(2)	6.2(5)	8
C6	0.4571(4)	0.27206(30)	0.20539(29)	0.585(2)	6.2(5)	16
C7	0.4676(4)	0.28646(30)	0.08329(29)	0.585(2)	6.2(5)	16
C8	0.1042(4)	0.2500	0.85259(29)	0.585(2)	6.2(5)	8
C9	0.4660(4)	0.18266(30)	0.13269(29)	0.585(2)	6.2(5)	16
C10	0.4587(4)	0.32056(30)	0.54849(29)	0.585(2)	6.2(5)	16
C11	0.0000	0.27296(30)	0.44509(29)	0.585(2)	6.2(5)	8
C12	0.8519(4)	0.2500	0.40169(29)	0.585(2)	6.2(5)	8

obtained were $a = 13.71119(16)$, $b = 22.2688(5)$, $c = 20.2631(6)$ Å. The final atomic positions and isotropic displacement parameters are listed in Table 5 with the final Rietveld plot displayed in Figure 9. The average T−O bond length (1.649 Å) and average O−T−O and T−O−T angles (104.9 and 145.6°, respectively) were found to be in good agreement with those expected for zeolitic materials. We also note that during the difference Fourier map analysis, the O11 atom was positioned in a rather disordered manner, which led us to include another oxygen atom (i.e., O22) in the refinement. This resulted in a notable improvement on the fitting quality; the R_F was decreased from 7.39 to 2.87%. The final refined structure of as-made Li-Al-EU-1 along the *a*-axis is shown in Figure 10. Here framework oxygen atoms and organic SDA molecules have not been included for clarity. When the structure was refined in the space group *Cmme*, the occupancy at site T9, which is indicated by

dx.doi.org/10.1021/ja1095057 |*J. Am. Chem. Soc.* 2011, 133, 1917–1934

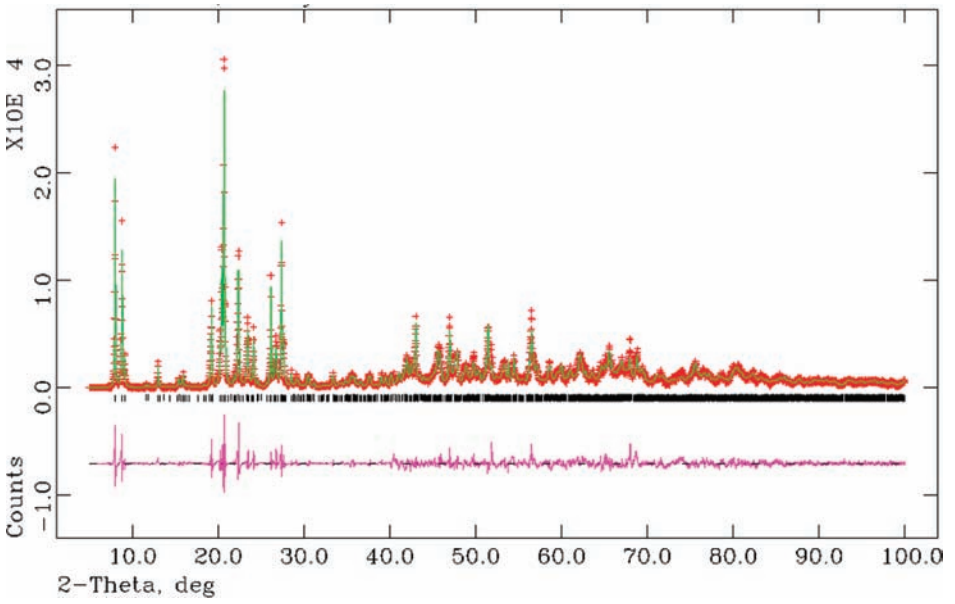

Figure 9. Rietveld plot for as-made Li-Al-EU-1: observed (crosses), calculated (solid line), and difference (lower trace) powder synchrotron diffraction patterns. The tick marks indicate the positions of allowed reflections. The 2θ range higher than 40° has been scaled up by a factor of 5 to show more detail.

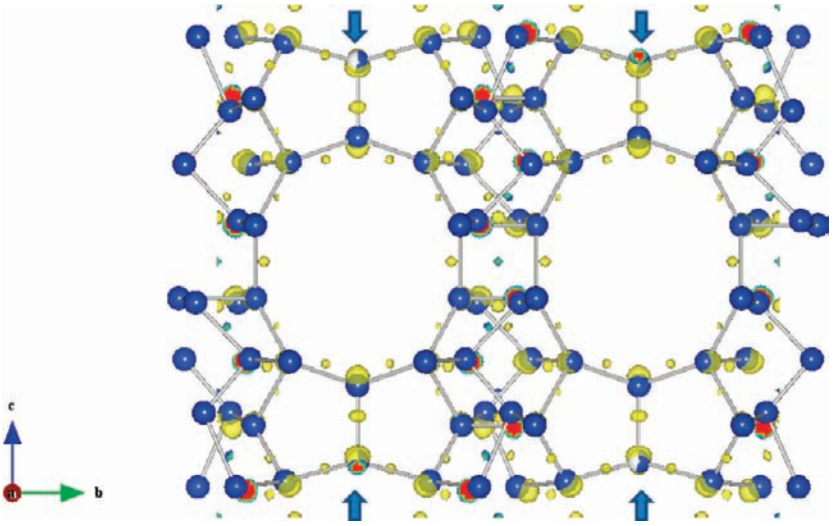

Figure 10. The framework structure of as-made Li-Al-EU-1 with the electron density taken from the powder charge-flipping map. Framework oxygen atoms and HM^{2+} molecules have been omitted for clarity. The framework defect sites caused by Li substitution are indicated by arrows.

arrows in Figure 10, was converged to 0.583, indicating the presence of 4.7 Si atoms at this site, unlike the case of the other 9 T-sites characterized by an occupancy of 1 in all (Table 5). Assuming that the rest of site T9 are occupied by Li atoms, the number (3.3) of its framework Li atoms was calculated to be more than twice larger than the value (1.5) per unit cell inferred from elemental analysis. However, Rietveld analysis of the synchrotron diffraction data for as-made Li-Al-EU-1 clearly shows the nonrandom distribution of Li atoms over its 10 different T-sites.

On the other hand, Rietveld analysis of the synchrotron diffraction data for as-made Na-Al-EU-1 gave a satisfactory R_{wp} value of 5.89%. The final unit cell parameters obtained were a = 13.70470(27), b = 22.22854(32), c = 20.27457(29) Å. The final atomic positions and isotropic displacement parameters and the final Rietveld plot for this conventional EU-1 zeolite can be found in Supporting Information Table S2 and Figure S8, respectively. Like for the case of as-made Li-Al-EU-1, some disorder in positions O11 and O14 was observed from the difference Fourier map analysis. Again, inclusion of two O22 and O23 atoms corresponding to the disordered missing oxygen atoms gave a notable decrease in R_F value (Supporting Information Table S1). The average T−O bond length was determined to be 1.623 Å, and the average O−T−O and T−O−T angles 105.8 and 150.5°, respectively. Unlike the case of as-made Li-Al-EU-1, however, the pCF analysis showed no signs of the presence of framework defects with the reduced electron density in as-made Na-Al-EU-1 (Supporting Information Figure S9), suggesting that all T-sites in this material are fully occupied by Si and Al.

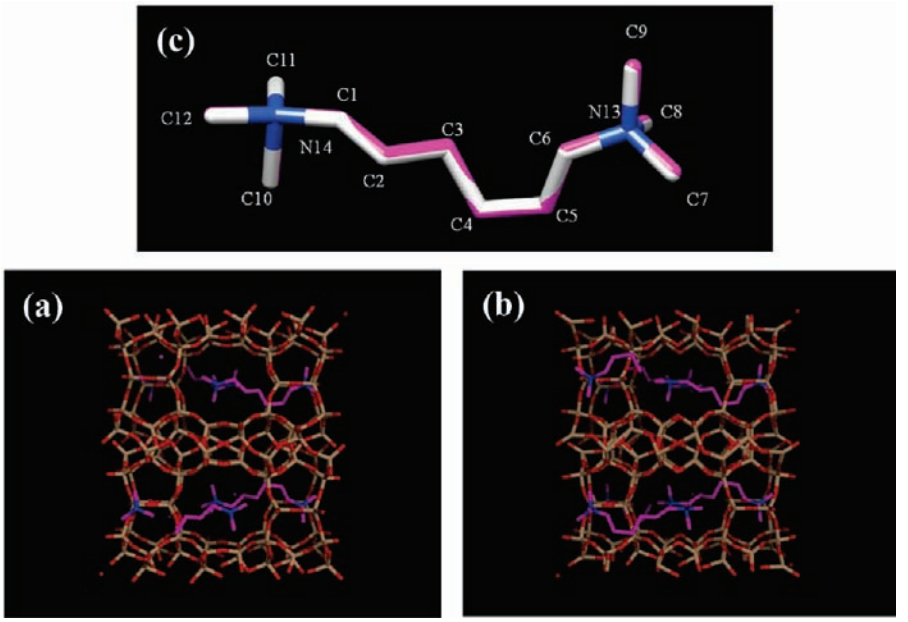

Figure 11. Energy-minimized conformations for the HM^{2+} ions within the 10-ring channel with large side pockets down the *a*-axis in as-made Li-Al-EU-1: (a) initial structure obtained from the global optimization using the parallel tempering method and (b) final structure from Rietveld refinements. The symmetry of HM^{2+} ions only has been reduced from *Cmme* to $P2_12_12$ for clarity. Panel c shows the difference in the initial and final structures of the occluded HM^{2+} cation which are represented by gray-white and pink sticks, respectively.

Figure 11 shows the energy-minimized conformations for the HM^{2+} ions within the 10-ring channel with large side pockets in as-made Li-Al-EU-1. To maintain a sensible model, C−C and C−N bond distances in the organic SDA molecule were constrained to 1.54(5) and 1.47(5) Å, respectively. Assuming the space group *Cmme*, no significant alterations in their conformation were found during the refinement. However, we found that the conformation of the occluded HM^{2+} ions alternates along the *c*-axis so that they show a face-to-face arrangement in the 10-ring window. It is interesting to note here that the C_4-C_5 bond in the central hexamethylene chain adopts a gauche configuration, while the other four C−C bonds in the corresponding chain do a trans conformation. Figure 11 also shows no significant differences in the initial structure obtained from the global optimization based on the parallel tempering algorithm and the final structure from Rietveld refinements, suggesting that HM^{2+} ions are, to some extent, ordered within the large cavities of Li-Al-EU-1. However, this is not the case of the organic guest molecules in as-made Na-Al-EU-1, because we were not able to reasonably locate their positions by the combined use of global optimization and Rietveld refinement methods.

The synthesis results in Table 1 demonstrate that the zeolites obtained with no noticeable impurities in the presence of Li^+ ions under the synthesis conditions studied here also include Li-Al-UZM-9, Li-Al-UZM-22, and Li-Al-sodalite. Unlike the spectrum of as-made Li-Al-EU-1, however, none of the ^{29}Si MAS NMR spectra of the as-made form of these three zeolites, which were prepared in the TEA^+-TMA^+ or TEA^+-HM^{2+} double-organic additive system, exhibited a noticeable ^{29}Si resonance around −90 ppm attributable to the presence of framework Li atoms. This indicates that the synthesis of `lithoaluminosilicate' Li-Al-EU-1 is not solely due to the application of the CDM approach to zeolite synthesis, although this new synthetic strategy proved fruitful for expanding the compositional regime of crystalline microporous materials.[2,3] To check whether other structure types of zeolites with lithoaluminosilicate and/or lithosilicate compositions can be obtained, zeolite syntheses using a number of different linear, diqaternary alkylammonium ions such as crystallization organic SDAs in the Li^+-TEA^+ SDA system are currently underway in our laboratory.

CONCLUSIONS

A total of 40 pairs of aluminosilicate and gallosilicate zeolite synthesis runs have been carried out under 4 different CDM synthesis conditions in which the Si/Me ratio (Me = Al or Ga) is varied between $5 \leq Si/Me \leq 16$. We were able to obtain 11 different zeolite structures by varying the crystallization temperature and the type and/or amount of alkali metal cations employed as a crystallization SDA. Since only 5 out of 40 pairs of synthesis runs gave the same product selectivity, however, it is clear that the structure-directing abilities of Al and Ga are significantly different from one another even at intermediate-silica compositions. In many cases, in addition, the crystal morphology of zeolites prepared via a CDM approach is notably different from that of the corresponding materials synthesized by the conventional procedure. Unlike ZSM-18, UZM-22 shows no significant preference of Al substitution for site T1, mainly due to notable differences in the size and rigidity of organic SDAs used in the synthesis of these two MEI-type zeolites. In particular, the choline molecules in as-made UZM-22 have been characterized to exist as the gauche conformer stabilized by one intramolecular C−H···O hydrogen bond. By contrast, the EU-1 zeolite prepared using a lithium aluminosilicate in the TEA^+-HM^{2+} mixed organic system was found to have framework Li atoms that are nonrandomly distributed over the 10 crystallographically different tetrahedral sites, while being easily extracted from the EU-1 framework during the calcination step to remove the organic SDAs occluded.

■ ASSOCIATED CONTENT

Supporting Information. Complete ref 2a and additional information as noted in the text. This material is available free of charge via the Internet at http://pubs.acs.org.

■ AUTHOR INFORMATION

Corresponding Author
sbhong@postech.ac.kr

■ ACKNOWLEDGMENT

This work was supported by the National Research Foundation of Korea (R0A-2007-000-20050-0 and 2009-0092793) and by the Carbon Dioxide Reduction and Sequestration R&D Center (16-2008-02-005-01). The work at Pohang Acceleration Laboratory (PAL) was supported in part by the Ministry of Science and Technology of Korea and POSTECH. We thank the staffs at 8C2, PAL, for their assistance with the powder diffraction measurements and Dr. A. Vicente and Prof. Ch. Fernandez, Université de Caen, for ^{27}Al 3Q MAS NMR measurements.

■ REFERENCES

(1) (a) Davis, M. E. *Nature* **2002**, *417*, 813.(b) Camblor, M. A.; Hong, S. B. In *Porous Materials*; Bruce, D. W., Walton, R. L., O'Hare, D., Eds.; Wiley: Chichester, 2011; p 265.

(2) (a) Blackwell, C. S.; et al. *Angew. Chem., Int. Ed.* **2003**, *42*, 1737. (b) Lewis, G. J.; Miller, M. A.; Moscoso, J. G.; Wilson, B. A.; Knight, L. M.; Wilson, S. T. *Stud. Surf. Sci. Catal.* **2004**, *154*, 364. (c) Miller, M. A.; Moscoso, J. G.; Koster, S. C.; Gatter, M. G.; Lewis, G. J. *Stud. Surf. Sci. Catal.* **2007**, *170A*, 347. (d) Miller, M. A.; Lewis, G. J.; Moscoso, J. G.; Koster, S.; Modica, F.; Gatter, M. G.; Nemeth, L. T. *Stud. Surf. Sci. Catal.* **2007**, *170A*, 487.

(3) (a) Kim, S. H.; Park, M. B.; Min, H.-K.; Hong, S. B. *Microporous Mesoporous Mater.* **2009**, *123*, 160. (b) Lee, J. H.; Park, M. B.; Lee, J. K.; Min, H.-K.; Song, M. K.; Hong, S. B. *J. Am. Chem. Soc.* **2010**, *132*, 12971.

(4) (a) Park, S.-H.; Parise, J. B.; Gies, H.; Liu, H.; Grey, C. P.; Toby, B. H. *J. Am. Chem. Soc.* **2000**, *122*, 11023. (b) Park, S. H.; Daniels, P.; Gies, H. *Microporous Mesoporous Mater.* **2000**, *37*, 129. (c) Cheetham, A. K.; Fjellvag, H.; Gier, T. E.; Kongshaug, K. O.; Lillerud, K. P.; Stucky, G. D. *Stud. Surf. Sci. Catal.* **2001**, *135*, 158. (d) Burton, A. W.; Zones, S. I.; Elomari, S. *Curr. Opin. Colloid Interface Sci.* **2005**, *10*, 211.(e) Davis, M. E.; Zones, S. I. In *Synthesis of Porous Materials*; Occelli, M. L., Kessler, H., Eds.; Marcel Dekker: New York, 1997; p 1. (f) Corma, A. In *Proceedings of the 14th International Zeolite Conference*, Cape Town, April 25−30, 2004; van Steen, E., Callanan, L. H., Claeys, M., Eds.; Document Transformation Technologies: Cape Town, 2004; p 25.

(5) (a) Krutskaya, T. M.; Kolishev, A. N.; Morozkova, V. E.; Berger, A. S. *Zh. Neorg. Khim.* **1985**, *3*, 783.(b) Vaughan, D. E. W.; Strohmaier, K. G. U.S. Patent 5,096,686, 1992.(c) Hong, S. B.; Kim, S. H.; Kim, Y. G.; Kim, Y. C.; Barrett, P. A.; Camblor, M. A. *J. Mater. Chem.* **1999**, *9*, 2287. (d) Cho, H. H.; Kim, S. H.; Kim, Y. G.; Kim, Y. C.; Koller, H.; Camblor, M. A.; Hong, S. B. *Chem. Mater.* **2000**, *12*, 2292.

(6) Strohmaier, K. G.; Vaughan, D. E. W. *J. Am. Chem. Soc.* **2003**, *125*, 16035.

(7) (a) Warrender, S. J.; Wright, P. A.; Zhou, W.; Lightfoot, P.; Camblor, M. A.; Shin, C.-H.; Kim, D. J.; Hong, S. B. *Chem. Mater.* **2005**, *17*, 1272. (b) Han, B.; Shin, C.-H.; Warrender, S. J.; Lightfoot, P.; Wright, P. A.; Camblor, M. A.; Hong, S. B. *Chem. Mater.* **2006**, *18*, 3023.

(8) Casci, J. L.; Lowe, B. M.; Whittam, T. V. U.S. Patent 4,537,754, 1985.

(9) *X'pert HighScore Plus Program, Version 2.2*; PANanalytical, Almelo, Netherlands, 2002.

(10) Massiot, D. *J. Magn. Reson. A* **1996**, *122*, 240.

(11) Amoureux, J. P.; Fernandez, C. *Solid State Nucl. Magn. Reson.* **1998**, *10*, 211.

(12) (a) Frontera, C.; Rodriguez-Carvajal, J. *Physica B (Amsterdam, Neth.)* **2003**, *335*, 219. (b) Roisnel, T.; Rodriguez-Carvajal, J. *EPDIC 7, Proc. Eur. Powder Diffr. Conf., 7th, 2000, Part 1 and 2* **2001**, *378*−*3*, 118.

(13) (a) Cerny, R.; Favre-Nicolin, V. Z. *Kristallogr.* **2007**, *222*, 105. (b) Favre-Nicolin, V.; Cerny, R. *J. Appl. Crystallogr.* **2002**, *35*, 734.

(14) (a) Larson, A.; von Dreele, R. B. *General Structure Analysis System GSAS*; Los Alamos National Laboratory: Los Alamos, NM, 2000. (b) Toby, B. H. *J. Appl. Crystallogr.* **2001**, *34*, 210.

(15) (a) Hastings, J. B.; Thomlinson, W.; Cox, D. E. *J. Appl. Crystallogr.* **1984**, *17*, 85. (b) Finger, L. W.; Cox, D. E.; Jephcoat, A. P. *J. Appl. Crystallogr.* **1994**, *27*, 892.

(16) (a) Barrer, R. M. *Hydrothermal Chemistry of Zeolites*; Academic: London, 1989.(b) Hong, S. B.; Lear, E. G.; Wright, P. A.; Zhou, W.; Cox, P. A.; Shin, C.-H.; Park, J.-H.; Nam, I.-S. *J. Am. Chem. Soc.* **2004**, *126*, 5817.

(17) Wang, G.; Marler, B.; Gies, H.; Fyfe, C. A.; Sidhu, P.; Yilmaz, B.; Muller, U. *Microporous Mesoporous Mater.* **2010**, *132*, 43.

(18) Fricke, R.; Kosslick, H.; Lischke, G.; Richter, M. *Chem. Rev.* **2000**, *100*, 2303.

(19) International Zeolite Association, Structure Commision, http://www.iza-structure.org.

(20) O'Keeffee, M.; Hyde, B. G. *Acta Crystallogr.* **1978**, *B34*, 3519.

(21) Treacy, M. M. J.; Higgins, J. B. *Collection of Simulated XRD Powder Patterns for Zeolites*, 5th ed.; Elsevier: Amsterdam, 2007.

(22) Ahman, J.; Svensson, G.; Albertsson, J. *Acta Crystallogr.* **1996**, *C52*, 1336.

(23) (a) Camblor, M. A.; Hong, S. B.; Davis, M. E. *Chem. Commun* **1996**, 425. (b) Hong, S. B.; Camblor, M. A.; Davis, M. E. *J. Am. Chem. Soc.* **1997**, *119*, 761. (c) Kim, S. H.; Lee, J.; Cho, S. J.; Shin, C.-H.; Heo, N.-H.; Hong, S. B. *Microporous Mesoporous Mater.* **2008**, *114*, 343.

(24) (a) Aiello, R.; Barrer, R. M. *J. Chem. Soc. A* **1970**, 1470. (b) Bieniok, A.; Bornholdt, K.; Brendel, U.; Baur, W. H. *J. Mater. Chem.* **1996**, *6*, 271. (c) Quirin, J. C.; Yuen, L. T.; Zones, S. I. *J. Mater. Chem.* **1997**, *7*, 2489. (d) Barrett, P. A.; Valencia, S.; Camblor, M. A. *J. Mater. Chem.* **1998**, *8*, 2263. (e) Kim, S. H.; Kim, S. D.; Kim, Y. C.; Kim, C.-S.; Hong, S. B. *Microporous Mesoporous Mater.* **2001**, *42*, 121. (f) Itabashi, K.; Ikeda, T.; Matsumoto, A.; Kamioka, K.; Kato, M.; Tsutsumi, K. *Microporous Mesoporous Mater.* **2008**, *114*, 495.

(25) (a) Lillerud, K. P.; Raeder, J. H. *Zeolites* **1986**, *6*, 474. (b) Matijasic, A.; Patarin, J. *Microporous Mesoporous Mater.* **1999**, *29*, 405.

(26) (a) Fajula, F.; Vera-Pacheco, M.; Figueras, F. *Zeolites* **1987**, *7*, 203. (b) Maubert, A.; Dutartre, R.; Menorval, L.-C.; Figueras, F. *Zeolites* **1993**, *13*, 587.

(27) Inoue, T.; Itakura, M.; Jon, H.; Oumi, Y.; Takahashi, A.; Fujitani, T.; Sano, T. *Microporous Mesoporous Mater.* **2009**, *122*, 149.

(28) Hasha, D.; Sierra de Saldarriaga, L.; Saldarriaga, C.; Hathaway, P. E.; Cox, D. F.; Davis, M. E. *J. Am. Chem. Soc.* **1988**, *110*, 2127.

(29) (a) Vartuli, J. C.; Kennedy, G. J.; Yoon, B. A.; Malek, A. *Microporous Mesoporous Mater.* **2000**, *38*, 247. (b) Lee, S.-H.; Shin, C.-H.; Yang, D.-K.; Ahn, S.-D.; Nam, I.-S.; Hong, S. B. *Microporous Mesoporous Mater.* **2004**, *68*, 97.

(30) (a) Harmon, K. M.; Mounts, P. F. *J. Mol. Struct.* **1984**, *118*, 127. (b) Harmon, K. M.; Avci, G. F. *J. Mol. Struct.* **1984**, *118*, 267. (c) Harmon, K. M.; De Santis, N. J.; Brandt, D. O. *J. Mol. Struct.* **1992**, *265*, 47.

(31) (a) Behrens, P.; van de Goor, G.; Freyhardt, C. C. *Angew. Chem., Int. Ed.* **1995**, *34*, 2680. (b) Han, D.-Y.; Woo, A. J.; Nam, I.-S.; Hong, S. B. *J. Phys. Chem. B* **2002**, *106*, 6206.

(32) Lercher, J. A.; Jentys, A. *Stud. Surf. Sci. Catal.* **2007**, *168*, 435.

(33) Engelhardt, G.; Michel, D. *High-Resolution Solid-State NMR of Silicates and Zeolites*; Wiley: New York, 1987.

(34) Wölker, A.; Hudalla, C.; Eckert, H.; Auroux, A.; Occelli, M. L. *Solid State Magn. Reson.* **1997**, *9*, 143.

(35) Lawton, S. L.; Rohrbaugh, W. J. *Science* **1990**, *247*, 1319.

(36) Schmitt, K. D.; Kennedy, G. J. *Zeolites* **1994**, *14*, 635.

(37) Jacobsen, H. S.; Norby, P.; Bildsøe, H.; Jakobsen, H. J. *Zeolites* **1989**, *9*, 491.
(38) (a) Ciric, J. U.S. Patent 3,950,496, 1976. (b) Vaughan, D. E. W. U.S. Patent 5,976,491, 1999.(c) Afeworki, M.; Dorset, D. L.; Kennedy, G. J.; Strohmaier, K. G. *Stud. Surf. Sci. Catal.* **2004**, *154*, 1274.
(39) (a) Koelmel, C. M.; Li, Y. S.; Freeman, C. M.; Levine, S. M.; Hwang, M.−J.; Maple, J. R.; Newsam, J. M. *J. Phys. Chem.* **1994**, *98*, 12911. (b) Sabater, M. J.; Sastre, G. *Chem. Mater.* **2001**, *13*, 4520.
(40) Hong, S. B.; Cho, H. M.; Davis, M. E. *J. Phys. Chem.* **1993**, *97*, 1622.
(41) (a) Shantz, D. F.; Lobo, R. F. *J. Phys. Chem. B* **1998**, *102*, 2339. (b) Shantz, D. F.; Lobo, R. F. *Chem. Mater.* **1998**, *10*, 4015. (c) Shantz, D. F.; Fild, Ch.; Koller, H.; Lobo, R. F. *J. Phys. Chem. B* **1999**, *103*, 10858.
(42) (a) Koller, H.; Lobo, R. F.; Burkett, S. L.; Davis, M. E. *J. Phys, Chem.* **1995**, *99*, 12588. (b) Arnold, A.; Hunger, M.; Weitkamp, J. *Microporous Mesoporous Mater.* **2004**, *67*, 205. (c) Camblor, M. A.; Corma, A.; Valencia, S. *Microporous Mesoporous Mater.* **1998**, *25*, 59.
(43) Burton, A.; Accardi, R. J.; Lobo, R. F.; Falcioni, M.; Deem, M. W. *Chem. Mater.* **2000**, *12*, 2936.
(44) Park, S.-H.; Liu, H.; Kleinsorge., M.; Grey, C. P.; Toby, B. H.; Parise, J. B. *Chem. Mater.* **2004**, *16*, 2605.
(45) (a) McCusker, L. B.; Baerlocher, Ch.; Palatinus, L. *Z. Kristallogr.* **2007**, *222*, 47. (b) Palatinus, L.; Chapuis, G. *J. Appl. Crystallogr.* **2007**, *40*, 786.
(46) (a) Dorset, D. L.; Kennedy, G. J. *J. Phys. Chem. B* **2005**, *109*, 13891. (b) Xie, D.; McCusker, L. B.; Baerlocher, Ch.; Gibson, L; Burton, A. W.; Hwang, S. J. *J. Phys. Chem. C* **2009**, *113*, 9845.